

THE EFFECT OF SOLID MICRO PARTICLES ON MASS TRANSFER IN AGITATED DISPERSIONS

Minal Soni

2008

Submitted in fulfilment of the requirements for a Doctor of Philosophy degree in
Chemical Engineering, Faculty of Engineering, University of KwaZulu-Natal.

DECLARATION

I, Minal Soni, declare that:

1. The research reported, except where otherwise indicated, is my original work.
2. This thesis has not been submitted for a degree or examination at another university.
3. This thesis does not contain other persons' data, pictures, graphs or other information, unless acknowledged as being sourced from other persons.
4. This thesis does not contain other persons' writing, unless specifically acknowledged as being sourced from other researchers. Where other written sources have been quoted, then:
 - a. their words have been re-written but the general information attributed to them has been referenced;
 - b. where the exact words have been used, their writing has been placed inside quotation marks, and referenced.
5. The experimental data were measured at the Prague Institute of Chemical Technology during 2006 and 2007, where I attended as a Ph.D. student. The results were presented in Soni et al. (2006), Kordač and Linek (2006) and Linek et al. (2008).
6. This thesis does not contain text, graphics or tables copied and pasted from the Internet, unless specifically acknowledged, and the source being detailed in the thesis and in the References sections

Signed: _____

ACKNOWLEDGEMENTS

- The completion of this study would not have been possible without the assistance of Dr Michal Kordač and Prof Vaclav Linek of the Prague Institute of Chemical Technology (ICT). Despite testing their patience and goodwill, their commitment to my studies and their friendship always remained absolute. It was an honour to meet the people who do “the real science”.
- My gratitude to Profs Ramjugernath and Čarsky of UKZN for their guidance and assistance with funding.
- My mother, Shanta, who has always made my dreams her own regardless of the difficulties they brought. Nothing good in my life would be possible without her incredible support. The completion of this degree is dedicated to my mother and in memory of my late father, Vijay.
- My thanks to my wife, Vilosha, for her unselfish support, assistance and her patience.
- The financial assistance of Sasol and THRIP is gratefully acknowledged.
- Harko Mulder, Prathisha Devnarian and Craig McGregor of Sasol Technology for their assistance in allowing me to spend essential time at ICT.
- My colleagues Viran Pillay and Carl McCawley who understood due to shared pain. I appreciate their input and friendship. It was a pleasure working with them.
- The technical staff at UKZN who never turned me away. My thanks, in particular, to Mr Les Henwood who missed his calling to be a teacher.

ABSTRACT

The industrial application of gas-liquid contactors has made effective design and optimisation of these processes a very important topic. In order to sustain a competitive advantage, rate limiting steps must be clearly understood. Hydrodynamics, heat transfer and mass transfer are complicated features of gas-liquid contactors and require a fundamental understanding.

The mechanism of mass transfer in the presence of a small concentration of solid micro particles has been the subject of debate. The adsorption of gas by solid particles (“shuttle mechanism”) is the traditional explanation. Recent experimental evidence suggests that the introduction of micro particles removes trace surface active impurities from the system and allows the true mass transfer coefficient to be measured. The objective of this study was to confirm the surfactant removal theory. Mass transfer is a field characterised by imprecise empirical relationships and difficult to obtain experimental parameters. This puts into context the significant challenge posed in preparing the careful set of measurements and analyses presented in this study to lend support to the surfactant removal mechanism.

The study began with a review of mass transfer models. These models are based on concepts such as surface renewal and idealised turbulence. It is, however, difficult to choose between the models as they predict similar values despite being based on different mechanisms. The overall mass transfer coefficient is composed of the gas-phase coefficient ($k_G a$) and liquid-phase coefficient ($k_L a$). As the values of the coefficients are comparable and the solubility of oxygen or hydrogen is very low, the overall mass transfer coefficient is approximately equal to the liquid side coefficient. The relationship of k_L with the diffusion coefficient (D) is one of the limited ways of choosing between the models. Mass transfer models predict $k_L \propto D^n$. n is predicted

to be $\frac{2}{3}$ for a rigid surface (contaminated interface region) and $\frac{1}{2}$ for a mobile surface (clean interface region). If the surfactant removal mechanism applies, the introduction of solid particles will be accompanied by a reduction of n from $\frac{2}{3}$ to $\frac{1}{2}$.

The effect of particles on n can be calculated from precise measurement of k_L of gases with significantly different diffusion coefficients. A review of experimental methods was made to find precise methods to characterise mass transfer in the presence of solid micro particles. The chemical sulphite, gas-interchange and pressure step methods were identified as appropriate methods. These were implemented in a stirred cell (0.5 l) and an agitated tank (6 l).

The chemical sulphite measurements were used to confirm that the enhancement of $k_L a$ is due to an enhancement of k_L and not the specific interfacial area (a). Flat surface experiments were made using water and 0.8 M sodium sulphate batches. The reduction of n from $\frac{2}{3}$ to $\frac{1}{2}$ was confirmed in both apparatuses after the addition of solid particles. The data were very well correlated and the dependence of k_L on the energy dissipation rate per unit volume (e) is similar to the theoretically predicted value of $\frac{1}{4}$ for the exponent.

Observation of the reduction of n from $\frac{2}{3}$ to $\frac{1}{2}$ was extended to agitated dispersions. The stirred cell $k_L a$ data were measured by the gas interchange method and are of excellent quality. The agitated tank results were measured by pressure step methods. The pressure dependence of the polarographic probes affected the precision of the results and the effect was within the experimental uncertainty. The effect of particles on n could not, therefore, be conclusively confirmed in the agitated tank.

By relating precisely measured mass transfer coefficients to the diffusion coefficients; the surfactant removal theory is confirmed. The result is valid for a flat mass transfer area as well as for agitated dispersion where the nature of the interface region changes with time due to the accumulation of surfactants on an initially clean interface.

CONTENTS

DECLARATION	ii
ACKNOWLEDGEMENTS	iii
ABSTRACT	iv
CONTENTS	vi
LIST OF FIGURES	xi
LIST OF TABLES	xiv
NOMENCLATURE	xvi
Chapter 1 Introduction	1
Chapter 2 Theory	3
2.1. Basic concepts	4
2.2. Models of mass transfer	5
2.2.1. Film theory	5
2.2.2. Penetration and surface-renewal theory	7
2.2.3. Boundary layer theory	10
2.2.4. Idealized turbulence models	13
2.2.5. Eddy cell model (Lamont and Scott, 1970)	17
2.2.6. Bubble contamination kinetics (Alves et al., 2004)	20
2.2.7. Summary	22
2.3. Effects of solid micro particles	24
2.3.1. Hydrodynamic effect in the boundary layer	25

4.2.1.	Liquid batches	45
4.2.2.	Gases	47
4.2.3.	Solid particles	47
4.3.	Polarographic probes	47
4.3.1.	Measuring principle	48
4.3.1.1	Oxygen	48
4.3.1.2	Hydrogen	49
4.3.2.	Probe signal	49
4.3.2.1	Oxygen transport to the cathode	49
4.3.2.2	Limiting diffusion current region	50
4.3.3.	Materials of construction	52
4.3.3.1	Membrane material	52
4.3.3.2	Electrolyte	52
4.3.3.3	Anode	53
4.3.3.4	Cathode	53
4.3.4.	Signal linearity	54
4.3.5.	Transition characteristics	55
4.3.5.1	First Order response	56
4.3.5.2	Single layer model	58
4.3.5.3	Other models	58
4.3.6.	Pressure dependence	59
4.4.	Experimental techniques	60
4.4.1.	Surface sorption measurements	60
4.4.1.1	Measurements by the chemical sulphite method	60
4.4.1.2	Mass transfer coefficient (k_L)	61

6.4.2.	Agitated tank	108
6.4.2.1	Dynamic pressure method	108
6.4.2.2	Discrete dynamic method	111
6.5.	Chapter summary	113
Chapter 7	Conclusions	115
Chapter 8	References	117

LIST OF FIGURES

Figure 2-1: Diffusion across a thin film (unstirred layer) as idealised by the film theory - Cussler (1997)

Figure 2-2: A well mixed bulk region and a continuously renewed interfacial region (surface renewal theory) – Cussler (1997)

Figure 2-3: Formation of boundary layers when a sharp-edged plate is immersed in a stream of fluid – Cussler (1997)

Figure 2-4: Diagram to show the disintegration of non-isotropic large eddies into isotropic terminal eddies – Kawase and Moo-Young (1990)

Figure 2-5: Eddies bring fresh fluid to the surface - Lamont and Scott (1970)

Figure 2-6: Illustration of the small scale eddies superimposed on the fluid flow – Lamont and Scott (1970)

Figure 2-7: Idealised viscous eddy cell as presented by Lamont and Scott (1970)

Figure 2-8: Accumulation of surfactants on the bubble surface and movement of the contaminants to the bottom of the bubble

Figure 2-9: Concentration gradient at the interface for absorption with chemical reaction – Deckwer (1985)

Figure 2-10: Illustration to show the effect of reaction rate on absorption rate for a given set of experimental conditions (impeller speed, etc.) – Linek and Vacek (1981)

Figure 4-1: Stirred cell used for mass transfer measurements

Figure 4-2: Flow diagram of agitated tank used to measure k_L

Figure 4-3: Illustration of the construction of the polarographic probe

Figure 4-4: Transport zones of oxygen from the bulk to cathode – Linek et al. (1988)

Figure 4-5: Illustration of a polarogram indicating the various regions of probe operation – Linek et al. (1988)

Figure 6-8: Volumetric mass transfer coefficients measured in sulphate solution-gas dispersion in a stirred cell at 20 °C

Figure 6-9: Comparison of the effect of particle addition using Llorens et al. (1988) surface pressure interpretation

Figure 6-10: Graphs to show the effect of the pressure step and the model fit to the data

Figure 6-11: Volumetric mass transfer coefficients measured in the agitated tank by the dynamic pressure method

Figure 6-12: Volumetric mass transfer coefficients measured in the agitated tank by the discrete dynamic method (average of two batches)

LIST OF TABLES

Table 2-1: Predicted values of the exponent of diffusion coefficient (n) by mass transfer models

Table 2-2: Reaction rate regions for gas absorption with accompanied chemical reaction

Table 4-1: Diffusion coefficients for oxygen and hydrogen into pure water

Table 4-2: Liquid density, viscosity and surface tension values

Table 4-3 Table to show the materials of construction and applied potential of the polarographic probes

Table 4-4: List of chemisorption experiments made in this study to measure the effect of particles on reaction kinetics and interfacial area

Table 4-5: List of surface sorption experiments made in this study to determine the effect of particles on n

Table 4-6: List of experiments made in this study to determine the effect of particle addition on n in the stirred cell

Table 4-7: List of experiments made in this study to determine the effect of particle addition on n in the agitated tank

Table 5-1: Stirred cell specific O_2 absorption rates into 0.8 M Na_2SO_3 at 30 °C

Table 5-2: O_2 absorption rate into 0.8 M sulphite solution (without activated carbon particles) measured in the agitated tank at 30 °C and a gas flow of 1 l/min

Table 5-3: O_2 absorption rate into 0.8 M sulphite solution (with 1 g /l of activated carbon) measured in the agitated tank at 30 °C and a gas flow of 1 l/min

Table 5-4: Mass transfer coefficients measured in water at 20°C (with and without 1 g /l carbon) by surface desorption in the stirred cell

Table 5-5: Mass transfer coefficients measured in water at 30°C (with and without 1 g /l carbon) by surface desorption in the stirred cell

NOMENCLATURE

a	specific interfacial area based on the liquid volume, $\text{m}^2 \cdot \text{m}^{-3}$
A	area parameter used to account for side polarographic probe diffusion
A_{1-3}	constants in $k_L a$ correlation (Equation 6-4)
c_i	concentration in interface region, $\text{mol} \cdot \text{dm}^{-3}$
c^*	equilibrium concentration, $\text{mol} \cdot \text{dm}^{-3}$
c_P	concentration in as read by the polarographic probe, $\text{mol} \cdot \text{dm}^{-3}$
C_{surf}	surfactant concentration in the interface region, $\text{mol} \cdot \text{dm}^{-3}$
d	bubble diameter, m
D	gas diffusion coefficient in liquid, $\text{m}^2 \cdot \text{s}^{-1}$
e	power dissipated by agitator per unit volume of liquid, $\text{W} \cdot \text{m}^{-3}$
E	mass transfer enhancement factor
E_{SR}	residence time distribution used for surface renewal theory
f	agitator frequency, s^{-1}
F	agitator frequency, rpm
g	gravitational constant, $\text{m} \cdot \text{s}^{-2}$
ΔG	free energy of activation, $\text{J} \cdot \text{mol}^{-1}$
h_{trans}	height of clean segment at the point of mobile to rigid transition, m
h	Planck's constant, $6.626 \times 10^{-34} \text{ J} \cdot \text{s}$
H	normalized probe signal
I	signal of polarographic probe, V
ΔI	signal difference at time t and $(t + \Delta t)$, V
k_L	liquid-side mass transfer coefficient, $\text{m} \cdot \text{s}^{-1}$
$k_L a$	volumetric mass transfer coefficient, s^{-1}
k_m	first order probe constant, s^{-1}
k	single layer model probe constant, s^{-1}
l	liquid phase film thickness, m

Chapter 1 Introduction

The importance of the chemical and petrochemical industries to the global economy can not be overstated. Bubble column technology is at the core of many industrial processes. These reactors have no mechanical moving parts and have good heat and mass transfer properties. Research on gas-liquid contactors, which traditionally found relevance in biotechnological applications, is being directed towards chemical processing related applications.

Gas-liquid contactors provide scope for a wide range of research, such as, an understanding of the complex hydrodynamic, mass transfer and heat transfer properties. These phenomena are complicated by the addition of solid particles, which are frequently present in the dispersion as catalysts. While reliable mass transfer properties are crucial for correct sizing of the contactor, it is interesting to note that the mechanism of mass transfer under these conditions is still the subject of debate. The fundamental understanding of this mechanism, therefore, presents an opportunity to optimise commercially important processes.

The particular mass transfer phenomenon that has sparked interest in this fundamental study is the increase of mass transfer rate after the addition of solid micro particles. The traditional explanation is that mass transfer is enhanced due to a “shuttle mechanism” that assists gas to liquid transfer by adsorption. Kaya and Schumpe (2005) have presented evidence, which suggests that the mass transfer rate observed in the presence of micro particles is in fact the true mass transfer coefficient. The

Chapter 2 Theory

Mass transfer is a process due to both convection, which occurs on the macro scale and diffusion, which occurs on the micro scale. While it is easy to produce convection, diffusion is a spontaneous process that leads to homogenisation due to random molecular motion driven by concentration gradients. Diffusion proceeds at a relatively slow rate and is often the rate limiting step in distributing mass in the boundary region.

Of key interest in this study is that diffusion is responsible for gas absorption. The rate of the gas absorption process is accelerated by agitation. Diffusion still depends on random molecular motions over small distances; however, the stirring is a macroscopic process, which moves portions of liquid over much larger distances. Diffusion mixes newly adjacent portions and thus absorption occurs very much faster.

Mass transfer models (which describe gas absorption) also consist of two parts, i.e. (1) diffusion which is superimposed on (2) fluid flow. These models use convection to account for mixing in the bulk phase, while resistance to diffusion is limited to a thin layer at the phase interface. The solutes are assumed to be sparingly soluble, which allows diffusion induced convection to be neglected.

A review of these models is made in this chapter. This shows that the fluid flow assumption made during the derivation affects the influence that the diffusion coefficient has on the model prediction. These assumptions relate directly to the state

Equation 2-3 assumes that we correctly know the mass transfer driving force and that the activity coefficients tend to 1. The mass transfer coefficient, k_L , characterises the proportionality of flux with concentration difference. Further, models for the physical interpretation of the mass transfer coefficient are presented. The models are based on various combinations of convective and molecular diffusion motion. They describe the effect of molecular motion by molecular diffusion coefficients and the convective motion is described by various parameters. These parameters must be determined empirically as they usually have a relationship to well defined physical quantities.

Diffusion coefficients allow one to represent results in a general and more fundamental way. However, experimental limitations often make mass transfer coefficients a more practical approach. The approximation that the flux is proportional to the concentration difference is not always true. However, in the context of this study we are able to use the mass transfer approach successfully.

2.2. *Models of mass transfer*

An interface region is assumed to exist between the gas-liquid and liquid-gas phase boundaries. The gas phase resistance to mass transfer is usually negligible for absorption of a sparingly soluble solute such as oxygen. Mass transfer is a complex phenomenon, which is a result of fluid flow near the phase boundary as well as solute diffusion into this interface region. Most of the classical models use a concept of a stationary fluid, which allows for a simple solution of the diffusion equation. With progress in computation techniques, models including some kind of liquid motion have appeared.

2.2.1. Film theory

The model proposed by Nernst in 1904 (described by Cussler, 1997) is the simplest interfacial region model. The film theory is an example of a classical model.

A hypothetical stagnant film (shown in Figure 2-1) is assumed to exist at the phase boundary. By making this assumption, no fluid flow occurs at the interface and it is assumed that steady-state diffusion occurs across the film.

$$k_L = \frac{D}{l}$$

Equation 2-6

The film theory gives a simple physical picture of how mass transfer resistance can occur at the phase boundary. It is the first concept taught when introducing mass transfer as an academic study and is the basis used by many researchers to develop their ideas. It is implied in many mass transfer correlations as they are presented in terms of the Sherwood number. Despite the simplicity of the film model, it has remarkable success in predicting mass transfer changes for chemisorption and in concentrated solutions.

2.2.2. Penetration and surface-renewal theory

The surface-renewal theory was proposed by Higbie for a constant contact time (referred to as the penetration theory) and developed by Danckwerts in 1951 (Cussler, 1997). According to the theory, mass transfer is due to unsteady diffusion of solute into an element, which is exposed to the surface for a limited contact time, after which, the surface is renewed. Danckwerts extended the idea assuming equal probability of renewal of all surface elements. The element is exposed to the surface for a specific contact time, during which, diffusion into the element occurs. Figure 2-2 shows the concentration profile changing in time and the return of the element to the bulk liquid. The process is characterised by τ , which is an average residence time for an element in the interfacial region.

When the surface is quickly renewed and τ is small, the flux in the interfacial region is given by that for diffusion into an infinite slab. The renewal of the interfacial region occurs quickly and behaves like a thick film (Cussler, 1997). Transfer of interfacial elements is random and any surface element is equally likely to be withdrawn from the bulk phase. Unlike the film model, free movement of the interface occurs.

$$\begin{aligned} x = 0 & \quad c_1 = c_{1i} \\ x \rightarrow \infty & \quad c_1 = c_{bulk} \end{aligned}$$

Higbie's penetration theory assumes that the process is characterised by a single contact time:

$$N_1 = 2\sqrt{\frac{Du_{\max}}{\pi L}}(c_{1i} - c_1)$$

Equation 2-8

where, $\frac{L}{u_{\max}}$ is the contact time. Comparing Equation 2-8 to the Equation 2-3 we obtain for the mass transfer coefficient:

$$k_L = 2\sqrt{\frac{Du_{\max}}{\pi L}}$$

Equation 2-9

Surface-renewal theory (Danckwerts) is an improvement of the penetration theory. Each surface element is assumed to be equally likely to be renewed. The residence time distribution of the surface elements is given by:

$$E_{SR}(t) = \frac{e^{-t/\tau}}{\tau}$$

Equation 2-10

The average flux is:

$$N_1 = \sqrt{\frac{D}{\tau}}(c_{1i} - c_1)$$

Equation 2-11

Comparing this to the Equation 2-3 we obtain for the mass transfer coefficient:

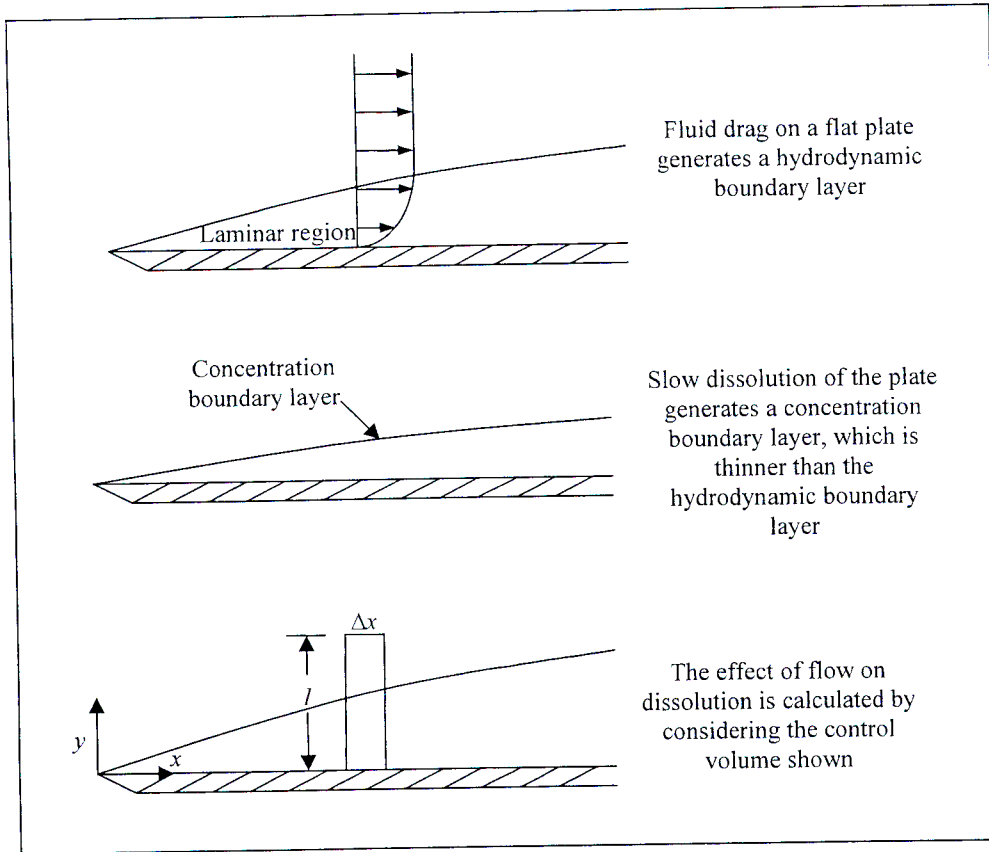


Figure 2-3: Formation of boundary layers when a sharp-edged plate is immersed in a stream of fluid – Cussler (1997)

The profile of the fluid flow parallel to the plate is assumed to be given by:

$$u_x = a_0 + a_1 y + a_2 y^2 + a_3 y^3 + \dots$$

$$u_y = 0$$

Equation 2-13

The parameters a_i are constant with respect to y but are functions of x . Cussler (1997) truncates Equation 2-13 to a third order equation and gives the following boundary conditions for flow:

$$\left(\begin{array}{ll} y = 0 & u_x = 0 \\ & \frac{\partial^2 u_x}{\partial y^2} = 0 \end{array} \right)$$

$$\left(\begin{array}{ll} y = \delta & u_x \approx u_0 \\ & \frac{\partial u_x}{\partial y} \approx 0 \end{array} \right)$$

$$N_1 = -D \frac{\partial c_1}{\partial y} \Big|_{y=0} = -Dc_{1i} \left[0 - \frac{3}{2} \left(\frac{1}{\delta_c} \right) + \frac{1}{2} \frac{3y^2}{\delta_c^3} \right]_{y=0} = \frac{3Dc_{1i}}{2\delta_c}$$

Equation 2-17

The rate at which the solute dissolves is given by:

$$N_1 = 0.323 \frac{Dc_{1i}}{x} \left(\frac{xu^0 \rho}{\mu} \right)^{1/2} \left(\frac{\mu}{\rho D} \right)^{1/3}$$

Equation 2-18

Comparison of the Equation 2-3 with Equation 2-18 and averaging over the length of the plate (L) results in the following relationship:

$$\frac{k_L L}{D} = 0.646 \left(\frac{Lu^0 \rho}{\mu} \right)^{1/2} \left(\frac{\mu}{\rho D} \right)^{1/3}$$

Equation 2-19

The boundary-layer theory is a more complete description of mass transfer as compared to the film and surface renewal models. Like other more complete models, it is based on parallels with fluid mechanics and heat transfer. It is applicable to specifically fluid-solid interfaces and the mathematics is more complicated. However, the fluid-solid interface gives insight into the behaviour of contaminated interface regions.

2.2.4. Idealized turbulence models

Kawase and Moo-Young (1990) present a review of mathematical models, which describe bioreactor design based on Kolmogoroff's theory of isotropic turbulence. Design parameters such as power input requirements, axial dispersion coefficients, mixing time, bubble size, gas hold-up, heat transfer and, most relevant to this study, mass transfer have been described by Kolmogoroff's theory.

$$\varepsilon = \mu^3 / \theta$$

Equation 2-20

A further hypothesis of Kolmogoroff is that an “inertial sub range” exists, where the energy spectrum is independent of ν and depends only on ε at infinite Reynolds number. The same amount of energy must be continuously drawn from the intermediate eddies as used to create smaller eddies at equilibrium. The Reynolds number for the intermediate eddies is high, therefore, it may be expected that the energy required to create small eddies is also independent of ν and will be of a similar form to Equation 2-20. The root-mean-square of the turbulence velocity between two points, which are a distance l apart is given by:

$$u \propto (\varepsilon l)^{1/3}$$

Equation 2-21

The significance of Kolmogoroff's theory is that the complex turbulence of gas-liquid systems can be described by a single parameter, ε . The above equations can be used to provide correlations for design parameters by a unified treatment for various phenomena as long as the liquid phase Reynolds number is sufficiently high for the inertial sub-range to exist in the energy spectrum. Kawase and Moo-Young (1990) report from their review of related literature that for gas-liquid two-phase flow, the energy input is mainly dissipated by a mechanism which is identical or very similar to that proposed by Kolmogoroff. Further, for flow fields that are non-isotropic and non-homogenous, the application of Kolmogoroff's theory as an approximate model has provided successful correlations.

The flow at the surface is modelled on the basis of the eddy structure of turbulence unaffected by surface tension. Higbie's penetration theory is used in conjunction with Kolmogoroff's theory of isotropic turbulence (which is used to calculate the velocity and scale of fluid flow in the interface region).

The relationship for velocity given in Equation 2-21 is applicable for both rigid and mobile surfaces; however, the proportionality constant is different. Kawase et al.

2.2.5. Eddy cell model (Lamont and Scott, 1970)

Lamont and Scott (1970) presented a model that assumes that the renewal of the surface is through the action of idealised small scale eddies of the turbulent field. The authors considered the case of a solid-liquid interface as well as gas-liquid interfaces. A key difference in the behaviour of a solid surface as compared to a gas surface is the hydrodynamic boundary condition at the interface.

Figure 2-5 illustrates motion of the eddies responsible for mass transfer. The fluid elements are brought to the surface, where they are deflected and return to the body of the fluid. Each motion brings fresh fluid to the surface so that mass transfer can occur by molecular diffusion.

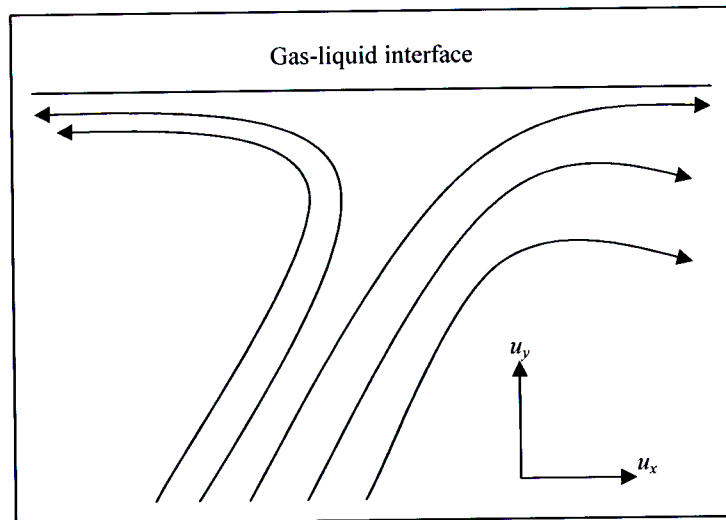


Figure 2-5: Eddies bring fresh fluid to the surface - Lamont and Scott (1970)

It is assumed that similar but very much smaller scale eddies are superimposed on the large eddies (see Figure 2-6). In the vicinity of the small eddy, mass transfer is controlled by the small scale turbulent motions if their energy is sufficiently large. For the case of a gas-liquid interface at a bubble surface, the prediction of the mass transfer coefficient is not affected by bubble size as the eddies are much smaller than the scale of the bubbles.

Velocity profiles are given in terms of stream functions for a square cell by Lamont and Scott for the free fluid and rigid interfaces.

The free fluid interface velocity profile is given in terms of the stream function:

$$\Psi = aA \left[0.0282 \frac{\pi}{a} y \cosh\left(\frac{\pi}{a} y\right) - 0.117 \sinh\left(\frac{\pi}{a} y\right) \right] \cos\left(\frac{\pi}{a} x\right)$$

Equation 2-26

The boundary conditions at the interface ($y = 0$) are:

$$u_y = 0 \quad \frac{\partial u_x}{\partial y} = 0$$

Unsteady-state diffusion as discussed in Section 2.2.2 is assumed and the final result for the free fluid case is:

$$k_L \propto \left(\frac{\mu}{D}\right)^{-1/2} (\varepsilon\mu)^{1/4}$$

Equation 2-27

The solid interface velocity profile is:

$$\Psi = a \left[\left(-0.124 - 0.0935 \frac{\pi}{a} y \right) \sinh\left(\frac{\pi}{a} y\right) + 0.124 \frac{\pi}{a} y \cosh\left(\frac{\pi}{a} y\right) \right] \cos\left(\frac{\pi}{a} x\right)$$

Equation 2-28

The boundary conditions at the interface ($y = 0$) are:

$$u_y = 0 \quad u_x = 0$$

The final result for the rigid interface is given by:

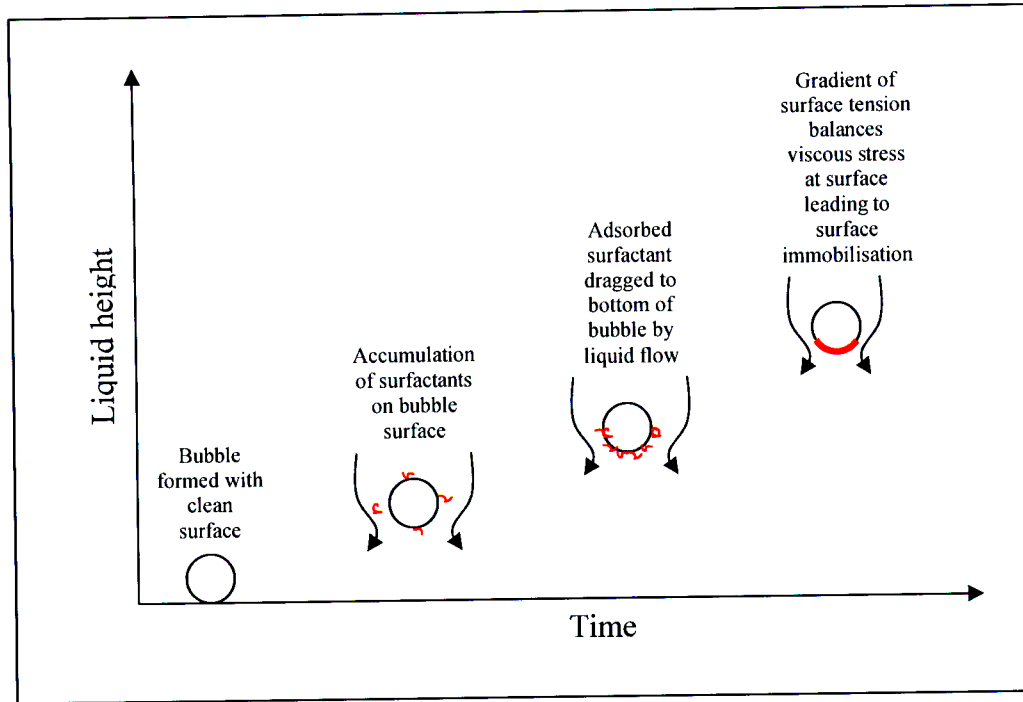


Figure 2-8: Accumulation of surfactants on the bubble surface and movement of the contaminants to the bottom of the bubble

The equations used to model the process are:

- Mobile interface region
Equation 2-8, which is derived from the penetration theory to describe the case of a mobile interface region.
- Rigid interface region
Equation 2-19, which is derived from the boundary-layer theory to describe the case of a rigid interface region.
- Mobile to rigid interface region transition
The following expression is used for the time a bubble spends having a mobile interface before becoming rigid (which depends on the bubble diameter and the concentration of the surfactants):

$$t^{mobile} = Const \frac{d^{1/2} \ln\left(\frac{d}{h_{trans}}\right)}{C_{surf}}$$

Equation 2-30

Where:

$$\left(\frac{\text{Sherwood}}{\text{number}} \right) = \text{Const} \left(\frac{\text{Reynolds}}{\text{number}} \right)^a \left(\frac{\text{Schmidt}}{\text{number}} \right)^b,$$

Equation 2-32

which implies that the mass transfer coefficient is a function of both flow and diffusion (Cussler, 1997). The principle interest of this study is the relationship between the mass transfer coefficient and the diffusion coefficient, which is written as follows:

$$k_L \propto D^n$$

The prediction of the value for n by the mass transfer models depends on the assumption of fluid flow at the interface. These predictions are summarised in the following table:

Table 2-1: Predicted values of the exponent of diffusion coefficient (n) by mass transfer models

Fluid flow at interface	Mass transfer model	n
1. No flow	• Film model	$n = 1$
2. Opposed flow	• Boundary-layer model • Eddy cell model – solid surface	$n = 2/3$
3. Opposed flow and free flow	• Bubble contamination kinetics	$1/2 \leq n \leq 2/3$
4. Free flow	• Surface renewal • Idealised turbulence model • Eddy cell model – fluid surface	$n = 1/2$

It is observed for the following assumptions that:

- No fluid flow at the interface

- Removal of surface-active material (Kaya and Schumpe, 2005).

2.3.1. Hydrodynamic effect in the boundary layer

Kluytmans et al. (2003) state that the interaction of particles with the gas-liquid interface can induce turbulence, which reduces the size of the effective boundary layer. The effect of the particles on the mass transfer coefficient tends to decrease at higher impeller speeds, due to increase in shear stress. Under these conditions, the effect of the particles is reduced. Kluytmans et al. (2003) indicate that the effectiveness of the particles to increase the mass transfer coefficient is determined by the particles hydrophobicity rather than the concentration of particles in the bulk liquid.

2.3.2. “Grazing” or “shuttle” mechanism

Kars et al. (1979) refer to a “grazing” effect, where the particles penetrate the interface and adsorb the gas solute. Alper et al. (1980) showed that fine quartz particles had no effect on the mass transfer coefficient, however, k_L increased in the presence of activated carbon particles. The effect was modelled in terms of a “shuttle” mechanism, where the small particles penetrate the interface, adsorb gas and release the solute after being returned to the liquid.

Due to the nature of the mechanism, a film model cannot be used to explain the phenomena (Beenackers and van Swaaij, 1993). The mechanism is explained as the transport of particles into the gas-liquid interface, adsorption of the gas solute and renewal of the particles. Models based on the “shuttle” mechanism predict a higher solid concentration at the interface than the bulk phase. The prediction is related to the wetting properties of activated carbon, which has a tendency to accumulate at a bubble surface (Beenackers and van Swaaij, 1993).

An expression for the enhancement factor (derived using penetration theory) is given by the following equation for a component A (Beenackers and van Swaaij, 1993):

- When the mass transfer coefficient reached a maximum value, successive measurements were made in the same batch. The coefficient was found to decrease after these repeated measurements.

Kordač and Linek (2006) have shown that the effect of particle addition on n can be measured using gases of different diffusion coefficients. This study presents measurements made across a flat mass transfer area as well as across bubble surfaces and the reduction of n after the addition of particles is shown.

2.4. *Gas absorption with chemical reaction*

Gas absorption with simultaneous chemical reaction allows for the measurement of mass transfer and interface properties (see Chapter 3). In order to implement these methods correctly, it is important to understand the kinetics of the reaction as the results are only meaningful if the measurements are made in the appropriate reaction rate regime. For example, the interfacial area can be calculated if the reaction rate is very much faster than the absorption rate.

2.4.1. Description of absorption with chemical reaction

The absorption rate can be increased when the absorbed species undergoes a chemical reaction. The concentration in the bulk liquid decreases, which increases the concentration difference, resulting in higher absorption rates (Deckwer, 1985). The process is described by the following equation:

$$N = k_L (c_1^* - c_1^{bulk}) = -D_1 \left(\frac{dc_1}{dx} \right)_{x=0}$$

Equation 2-34

Figure 2-9 shows the different concentration profiles at the interface based on the film model. The mass transfer coefficient remains unchanged while the concentration gradient becomes steeper due to faster reaction.

Figure 2-10 shows the dependence of absorption rate on the reaction rate. The curve is valid for changing reaction rate but for specific impeller speed, gas flow, etc. The effect on gas absorption is low when the chemical reaction rate is low. The enhancement factor in region III (referred to as the diffusion regime) is still unity.

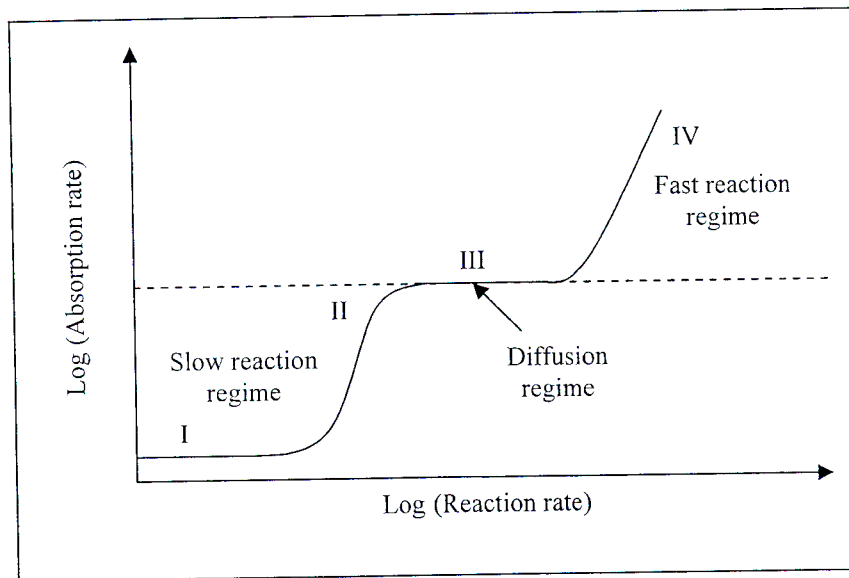


Figure 2-10: Illustration to show the effect of reaction rate on absorption rate for a given set of experimental conditions (impeller speed, etc.) – Linek and Vacek (1981)

The features of each of the regions shown in Figure 2-9 and Figure 2-10 are summarised in Table 2-2. In region IV the reaction proceeds regardless of the hydrodynamic conditions at the interface. The absorption rate is, therefore, dependent only on the interfacial area. In the region between III and IV, the effects of reaction and hydrodynamics on absorption are comparable.

be concluded that the kinetics are so sensitive to factors such as impurities, that unless a sulphite batch is identical, using the same kinetics can not be justified. The following factors were found to influence absorption rates:

- Sulphite concentration

The reaction can be assumed to be zero-order in sulphite concentration for solutions of concentration > 0.5 M (Linek and Vacek, 1981).

- Oxygen concentration

The order with respect to oxygen was found to depend on the interface concentration of oxygen as well as the purity of the sulphite solution (Linek and Vacek, 1981). The values reported in literature are as follows:

Concentration of $O_2 < 3.6 \times 10^{-4}$ M: *First order*

Concentration of $O_2 > 7 \times 10^{-4}$ M: *Second order*

For values in between the limits, it is advised to confirm the reaction order.

- Catalyst concentration

The reaction is generally accepted to be first-order.

- pH

The proposed relationship by Linek and Vacek (1981) is:

$$N \propto (pH - 7.9 + 0.04t)$$

Equation 2-37

, where t is the temperature in degrees Celsius.

2.5. Chapter summary

Mass transfer can be visualised in terms of simple physical models, where resistance to mass transfer occurs near an interface. These models consist of two parts, the first is an assumption of diffusion (using Fick's law) and the second is an assumption of fluid flow at the interface. The dependence of the mass transfer coefficient on the diffusion coefficient is given by the exponent n . For the case of no fluid flow at the interface (film model), n is predicted to be 1. When flow at the interface is opposed

Chapter 3 Experimental methods

The mass transfer coefficient (k_L) is a difficult parameter to measure directly. A more easily measured quantity is the volumetric mass transfer coefficient ($k_L a$), which is the product of k_L with the specific interfacial area (a). For the case of surface absorption (experiments with a flat mass transfer area) the parameter a is known exactly and hence k_L can be calculated. For the case of gas-liquid dispersion, there are limited methods for the measurement of a and the uncertainty associated with these measurements is large.

This chapter discusses principles for various methods for the measurement of $k_L a$, k_L and a . Precise and accurate values of these key parameters will assist in providing an understanding of the effect that the presence of solid micro particles have on mass transfer. The implementation of the techniques as well as the model equations are described at length in Chapter 4.

3.1. Methods of $k_L a$ measurement

Dynamic methods as well as chemical methods are discussed. Dynamic methods require a sudden change of concentration to be made whereas chemical methods require a source and a sink of the solute. Two types of liquid batches are considered

bubbles to leave the batch. Agitation is resumed and simultaneously the batch is aerated with a gas of different concentration.

The large variation of concentration of gases in individual bubbles (observed in the instantaneous method) is avoided in this way. A drawback of the method is that the initial part of the measurement is made while the dispersion is still developing. The k_La value measured is dependent on the development of the bubble distribution. For the case of coalescent batches the distribution develops quickly and the correct k_La value is measured. According to Linek et al. (1989) for non-coalescent batches this variation of the start-up method measures the initial k_La value (before full development of the gas hold-up). The uncertainty of the measurements made for non-coalescent batches is, therefore, slightly larger.

A variation of the start-up method, referred to as the standard method, is described by Linek et al. (1989). Dissolved gases are removed from the liquid batch by vacuum desorption. The batch is then aerated with pure oxygen. The method is used as a basis for comparison for other dynamic methods.

3.1.2. Dynamic pressure method (DPM)

For the dynamic pressure method (Linek et al., 1989) a step change in concentration is induced by making a step change in the system pressure. Other methods requiring a step-change (such as gas interchange) are affected by the finite rate of propagation of the change. The DPM changes the concentration of oxygen in all the bubbles simultaneously and is, therefore, not affected by non-ideal mixing in the gas phase. For the instantaneous interchange method, it is possible to obtain bubbles of pure nitrogen and bubbles of pure oxygen during the gas interchange (Linek et al., 1989). Since the effect of non-ideal mixing increases with increasing concentration difference, the DPM is preferred as the concentration difference between individual bubbles is small. Further, there is no interruption of the dispersion as in the start-up method.

Only a small but fast change in pressure is necessary (approximately 20%), which makes the method suitable for large-scale reactors. A model describing the

advantage over the DPM as the probe position does not influence the measured value. As required by the DPM, the analytical technique must not be pressure dependant.

3.1.4. Chemical method

Chemical methods use model systems, which enable measurement of k_L and or a . Vasconcelos et al. (1997), for example, discuss a steady-state method, which uses hydrogen peroxide. Oxygen is continuously generated in the liquid phase by the decomposition of hydrogen peroxide in the presence of a catalyst. The evolved gas is transferred into the gas phase. When the peroxide decomposition rate is equal to the rate of addition of peroxide, a steady-state is reached and $k_L a$ may be calculated.

Linek and Vacek (1981) describe the procedure used to determine the mass transfer coefficient using the chemical method (sulphite oxidation). Equations to calculate the absorption rate, N , were derived using the film model. With reference to the discussion in Section 2.4 (description of mass transfer with simultaneous chemical reaction), $k_L a$ and or a can be calculated if the experiment is performed in the appropriate reaction rate regime.

3.1.4.1 Determination of $k_L a$ in the diffusion regime

If the experiment is performed in Region III (see Figure 2-10) the effects of hydrodynamics and chemical reaction on the absorption rate are similar. The concentration of O_2 in the bulk liquid is zero, however, there is no significant reaction in the interface region. According to Linek and Vacek (1981), the following equation applies:

$$Na = c_{O_2}^* k_L a$$

Equation 3-1

$k_L a$ can, therefore, be determined by measuring the absorption rate and the solubility of O_2 .

where

$$X = \left(N_{cell}^2 \frac{(c_{tank}^*)^{n-1}}{(c_{cell}^*)^{n+1}} \right) \text{ and } Y = \left(\frac{\Phi_{tank}}{c_{tank}^* - c_{bulk}} \right)^2$$

Since the interfacial area is known for the stirred cell, N_{cell} can be measured and correlated in consideration of changes to pH and catalyst concentration. The overall absorption rate (Φ_{tank}) is also measurable. When the experiments are performed using the sulphite solution and under the same conditions of pH, temperature and catalyst concentration, a plot of Y vs. X enables measurement of $k_L a$ as well as a . The straight-line graph is referred to as the Danckwert's plot and the y-intercept is the square of $k_L a$.

3.2. *Methods of interfacial area measurement*

3.2.1. Chemical method

With reference to Figure 2-10, the influence of hydrodynamics on the absorption rate is suppressed when the chemical reaction is very fast (Region IV). The interfacial area can be calculated in the fast reaction region using two absorbers. The first absorber must have a known interfacial area (such as a stirred tank) and the experiment in the second absorber must be made using the same sulphite solution. Linek and Vacek (1981) show that the ratio of absorption rates is given by:

$$\frac{a_{cell}}{a_{tank}} = \frac{NA_{cell}}{NA_{tank}}$$

Equation 3-5

Where the absorption rates (NA) are measurable (A is the total interfacial area) and a_{cell} is known.

3.2.2. Optical method

Optical methods yield local information about the interfacial area. These methods involve light undergoing refraction, diffraction or reflection on the bubble surface

however, used to measure the effect of solid particle addition on interfacial area in this study.

Optical methods can be used to estimate the interfacial area of dispersion. The method measures bubble sizes close to the wall. Further it is not suitable when solid particles are present.

The accuracy of the experimental methods relies on correct measurement of the concentration driving force. The preferred method in this study was the use of polarographic probes. It is important to establish the dependence of the probe behaviour on pressure changes for the DPM and discrete dynamic methods. The construction and characteristics of the probes are summarised in Chapter 4.

Chapter 4 Experimental

Selected mass transfer measurement techniques were implemented in two scales of apparatuses. The description of the apparatuses and the detail of the implementation of the methods as used in this study are described in this chapter. Sorption experiments were carried out in a stirred cell and an agitated tank. The methods were chosen for their superior precision in mass transfer rate measurement based on the review of experimental methods in the previous chapter. The construction and characteristics of the polarographic probes used to measure dissolved gas concentration are also described in this chapter.

4.1. Apparatuses

4.1.1. Stirred cell

The stirred cell (shown in Figure 4-1) consists of a Perspex bottom and a stainless steel wall. The inner diameter was 112 mm and the vessel had six baffles. The liquid phase impeller was a 60 mm vaned disc. A two-paddle agitator on a common shaft stirred the gas phase. Liquid was circulated in the vessel's jacket to maintain a constant temperature. 500 ml of liquid was filled into the apparatus and the specific interfacial area was 19.5 m^{-1} when the surface absorption experiments were performed. The apparatus was used to make both surface experiments as well as measurements in dispersion, in which case the gas was introduced below the impeller.

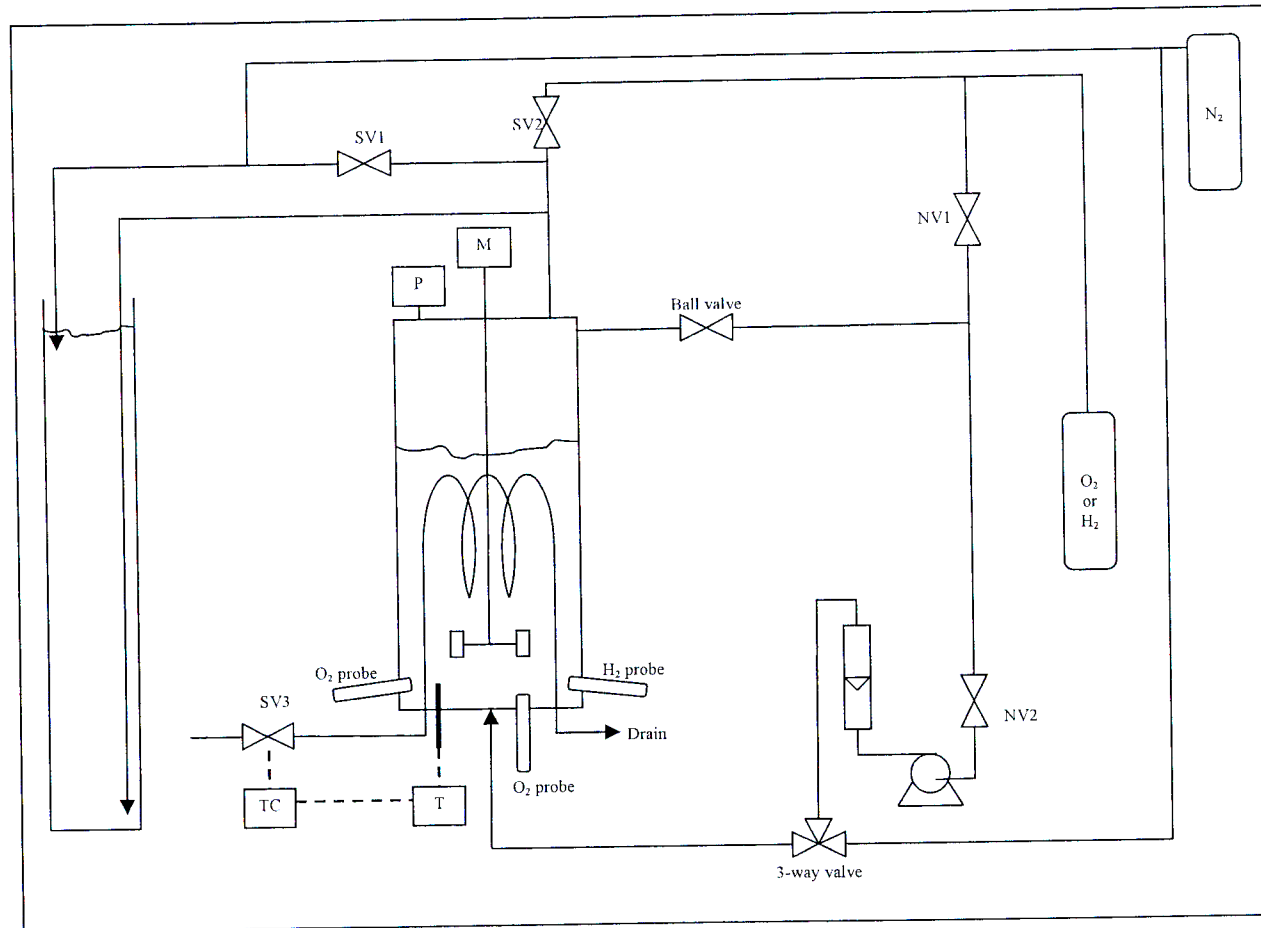


Figure 4-2: Flow diagram of agitated tank used to measure k_L

$$D = \left(\frac{\kappa}{h} \right) \left(\frac{V}{N_A} \right)^{\frac{2}{3}} T \exp \left(- \frac{\Delta G^*}{RT} \right)$$

Equation 4-1

N_A is Avogadro's number and ΔG^* the Gibb's free energy of activation of the diffusing solute in the electrolyte. The calculated values are shown in Table 4-1.

Table 4-1: Diffusion coefficients for oxygen and hydrogen into pure water

Solution	$D_{\text{Oxygen}} / \text{m}^2 \cdot \text{s}^{-1}$	$D_{\text{Hydrogen}} / \text{m}^2 \cdot \text{s}^{-1}$
Water (T = 20 °C)	2.10×10^{-9}	4.17×10^{-9}
Water (T = 30 °C)	2.74×10^{-9}	5.45×10^{-9}
0.8 M Sulphate (T = 20 °C)	1.80×10^{-9}	3.57×10^{-9}
0.8 M Sulphate (T = 30 °C)	2.37×10^{-9}	4.71×10^{-9}

Density, viscosity and surface tension of the solutions used in this study were measured and are presented in Table 4-2 (σ^f is the value in the presence of particles).

Table 4-2: Liquid density, viscosity and surface tension values

Solution	$\rho / \text{kg} \cdot \text{m}^{-3}$	$\mu / \text{mPa} \cdot \text{s}$	$\sigma / \text{mN} \cdot \text{m}^{-1}$	$\sigma^f / \text{mN} \cdot \text{m}^{-1}$
Water (T = 20 °C)	998.2	1.008	1.008	1.008
Water (T = 30 °C)	995.6	0.7977	0.7977	0.7977
Water (T = 25 °C)			71.26±0.11	71.47±0.13
0.8 M Sulphate (T = 20 °C)	1095	1.294	1.294	1.294
0.8 M Sulphate (T = 30 °C)	1089	1.100	1.100	1.100
0.8 M Sulphate (T = 25 °C)			72.64±0.32	74.02±0.0

The performance of the probe is very sensitive to both construction of the probe as well as preparation of the probe, especially with regards to fitment of the membrane. The probes used in this study are of a similar construction to that described by Linek et al. (1988). The construction of the hydrogen and oxygen probes is almost identical; therefore, much of the discussion that follows is about the oxygen probe.

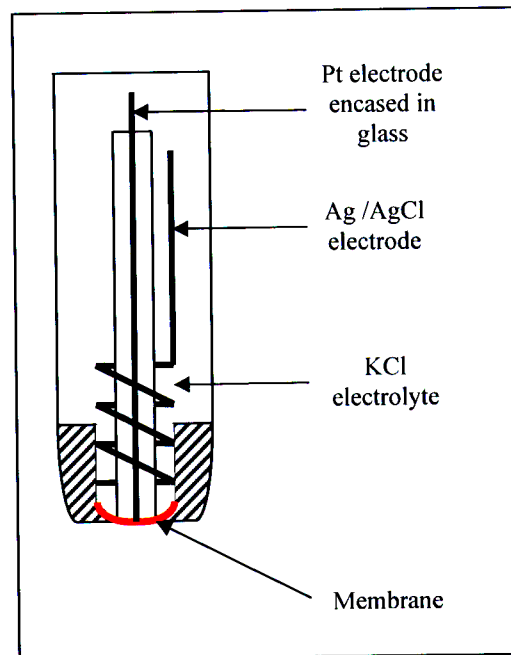


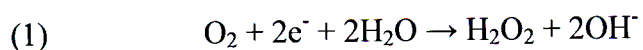
Figure 4-3: Illustration of the construction of the polarographic probe

4.3.1. Measuring principle

4.3.1.1 Oxygen

The measuring principle is described by Linek et al. (1988). A negative potential is applied to the cathode and dissolved O_2 concentration is reduced. The current flowing between the electrodes (probe signal) depends on rate of O_2 transport to the cathode as well reaction stoichiometry. The probe is operated such that the signal is controlled by O_2 diffusion rate towards the cathode and is thus a linear function of O_2 concentration.

The series of reactions at the cathode are complex but the following mechanism results:



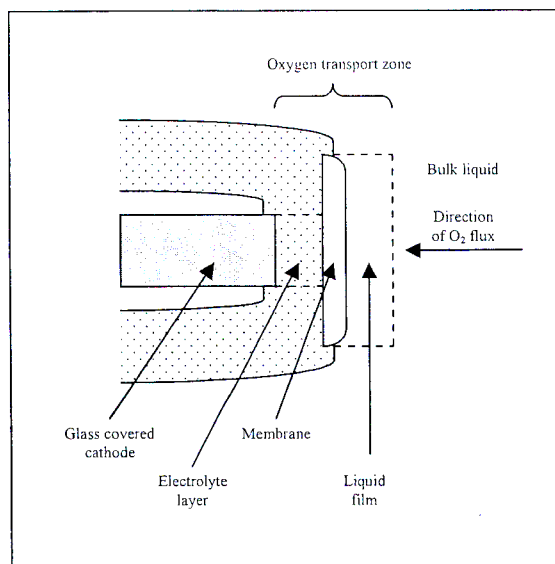


Figure 4-4: Transport zones of oxygen from the bulk to cathode – Linek et al. (1988)

4.3.2.2 Limiting diffusion current region

A polarogram is a plot of the probe signal as a function of the applied potential. It is important that the applied potential is chosen carefully as the probe signal is proportional to the concentration for only a particular range of potential. The polarogram (shown in Figure 4-5) consists of four regions (Linek et al., 1988):

- Region A
The signal is determined by the rate of electrochemical reduction of O_2 as the potential is below the decomposition potential for O_2 .
- Region B
The signal is determined by both the rate of O_2 reduction and the rate of transport to the cathode
- Region C – Limiting diffusion current region (LDCR)
The signal depends only on the rate of transport of O_2 as the reduction rate is very large compared to the rate of transport.
- Region D
The water decomposition potential is reached and H_2 is evolved.

The applied potential used for the hydrogen probe was +0.6 V. The potential for each probe was applied by a set of electronics that also converted the probe current signal into a volt signal, which was recorded by a data acquisition unit.

4.3.3. Materials of construction

Linek et al. (1988) discuss materials of construction for oxygen probes and their effect on probe operation. Some considerations are summarised below.

4.3.3.1 Membrane material

The membrane protects the electrodes from contamination by the test medium, it provides reproducible conditions for oxygen transport and minimises changes in the electrolyte composition. It must have selectivity for oxygen as opposed to gases such as CO₂ but a low permeability to allow four-electron stoichiometry to occur. Good mechanical strength, chemical inertness and physical properties that do not vary with time are also required.

Non-hydratable polymers such as PTFE and PP can be used, although they possess properties, which must be considered depending on the requirement of the probe. For example PTFE might be chosen over PP as it has a higher long term stability and higher thermal stability despite PP having a better selectivity to permeability ratio. T

The permeability of the membrane is also affected by the mechanical stress in the membrane, which means care must be taken when the membrane is fitted over the cathode. Hence probes prepared by different people following the same procedure can show different characteristics. 8 µm PP was used for the oxygen probes. A polymeric material called Saran was used for the hydrogen probes.

4.3.3.2 Electrolyte

The electrolyte permits transport of ions between the cathode and anode. The electrolyte must be free of impurities to ensure that there is no effect on the probe signal. 3 M KCl solution was used in this study.

Table 4-3 summarises the materials of construction for the probes used in this study. The hydrogen probe was identical in construction to the oxygen probe with two exceptions: (1) The electrical contacts are reversed, i.e. the applied potential is positive and (2) the membrane material was Saran.

4.3.4. Signal linearity

The signal linearity of the probes was tested by varying the partial pressure of the gases. Figure 4-7 shows the linear response of the oxygen probe over a wide concentration range. For these experiments the probes were immersed in a gas stream.

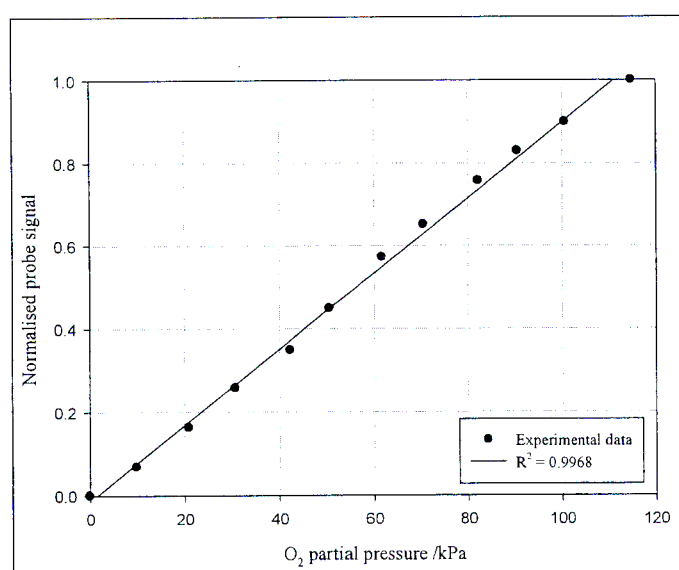


Figure 4-7: Linear response of the oxygen probe to a change in gas concentration

The signal of the hydrogen probe was also found to be linear in concentration. Figure 4-8 shows the linear behaviour when the gas concentration is increased. Figure 4-9 shows the behaviour for decreasing gas concentration. Both slopes are in agreement to within approximately 8%. Based on these results, the probes are well suited to measuring varying gas concentrations by monitoring the signal.

process under consideration approaches the rate of the probe response, the method becomes unsuitable for measurement of $k_L a$. The probes used in this study responded very quickly to changes in concentration, however, it is still necessary to understand the dynamics of the probe for the measurement of large mass transfer coefficients. For the dynamic pressure method, the dynamics of the probe are considered in order to extract the correct concentration-time profile from the probe signal.

4.3.5.1 First Order response

Sophisticated models exist for transition characteristics, however, for the purposes of this study it was sufficient to model the transition characteristic as a first order process:

$$\frac{dH}{dt} = -k_m H$$

Equation 4-2

, where H is the probe signal normalised between 1 and 0 using a linear transformation. The initial condition used to solve Equation 4-2 is:

$$t = 0, \quad H = 1$$

Solving Equation 4-2 results in the normalised probe signal described by:

$$H = \exp(-k_m t)$$

Equation 4-3

Figure 4-10 shows the response of an oxygen probe from pure oxygen to nitrogen:

- Figure 4-10A shows the measured signal response.
- Figure 4-10B shows the normalised signal as well as the model fit.
- Figure 4-10C shows the normalised response and model fit on a semi-log scale. The significance of this plot is that it shows a good fit to the measured data for 95% of the signal response.

4.3.5.2 Single layer model

Linek et al. (1988) present the following equation, which also describes the transition characteristics of a polarographic probe by a single parameter (k):

$$H(t) = 1 + 2 \sum_{n=1}^{\infty} (-1)^n \exp(kn^2 t)$$

Equation 4-4

The model is a simplification of the two region model described in the section that follows. The data fitted to the first order response model were also fitted to Equation 4-4 and are shown in Figure 4-11. The value of the objective function, which was minimised in order to make the fit, was similar to that of the first order model fit. This is further confirmation that the transition characteristics are well represented by Equation 4-3. The first order model fits were used in this study.

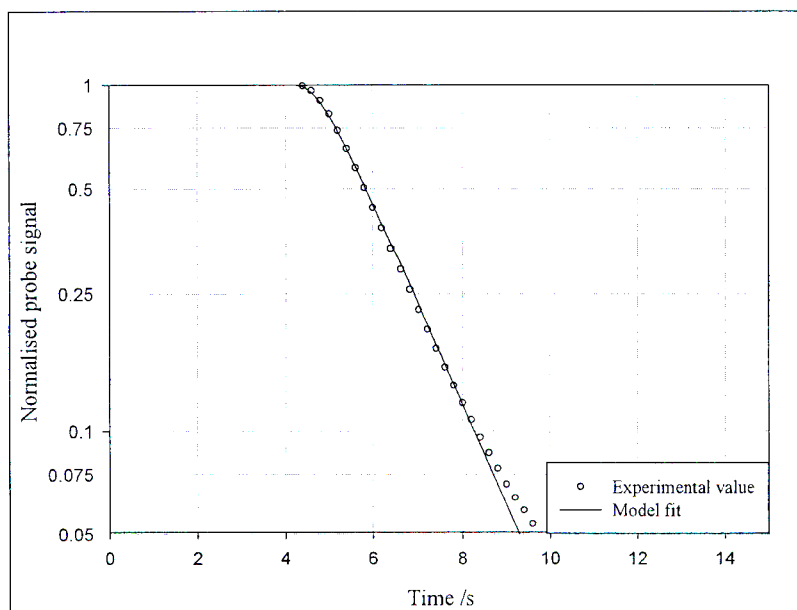


Figure 4-11: Normalised response and single-layer model fit on a semi-log scale.

4.3.5.3 Other models

Linek et al. (1988) present further models for transition characteristics. These models are suitable for probes that exhibit phenomena such as side diffusion. The approach of the dissolved gas through the membrane is not normal to the membrane, which results in tailing of the signal. The response of the probe is characterised by two k parameters

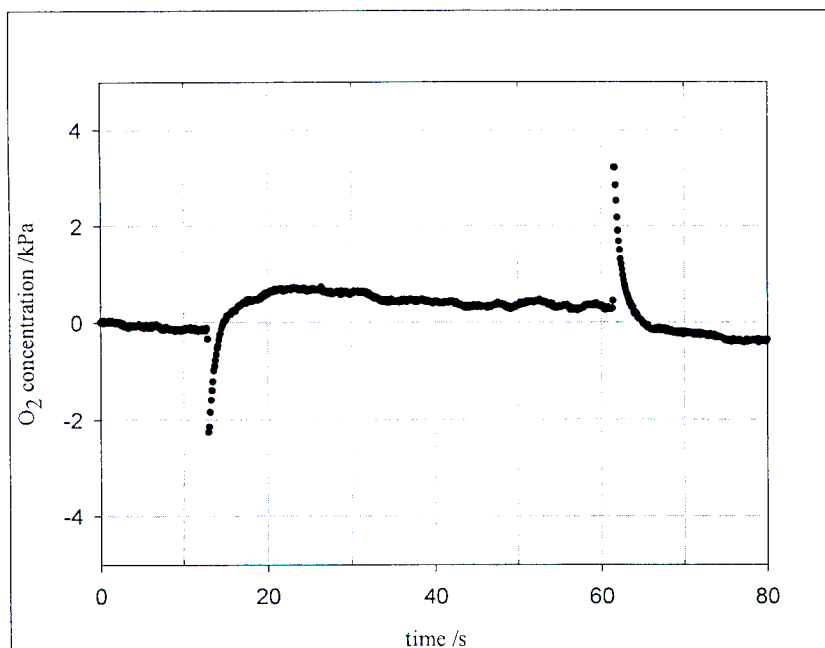


Figure 4-12: Response of an oxygen polarographic probe to a 20 kPa increase in pressure (at 13 s) and a pressure decrease (at 61 s)

4.4. *Experimental techniques*

4.4.1. Surface sorption measurements

Surface sorption measurements were made in the stirred cell using the chemical method and the gas interchange method. Sorption rates in the agitated tank were measured by the dynamic pressure method. This section details how the methods were implemented.

4.4.1.1 Measurements by the chemical sulphite method

Prior to using the chemical sulphite method for dispersion, it was necessary to investigate the influence of solid particles on the kinetics of the reaction. This will ensure that the correct absorption rates are calculated from the assumed kinetics. The absorption rate of O_2 in the presence of particles was measured in the stirred cell.

The stirred cell was equipped with a WTW pH meter (Type 538) as the kinetics are influenced by pH (see Section 2.4.2). The initial pH of the solution was between 9.5 and 9.6. The pH was adjusted to 8.5 using sulphuric acid. Cobalt sulphate solution

$$\frac{dc_L}{dt} = -k_L a c_L$$

Equation 4-7

Linek and Kordač (2006) have shown that if the probe signal is linear, $k_L a$ can be found using the following equation:

$$\ln(\Delta I) = -k_L a \Delta t + \text{const}$$

Equation 4-8

, where I is the probe signal and ΔI is the signal difference at time t and Δt . If $\ln(\Delta I)$ is plotted against t , the mass transfer coefficient is given by the slope. Since the interfacial area is known, k_L is calculated by dividing by the known interfacial area.

The DPM was used to measure desorption rates from the agitated tank. Although the concentration step was made using a pressure change, Equation 4-8 still applies. The tank was operated at the higher pressure (outlet opened to 2 m of water in the manostat) after saturating the batch. By opening SV1 (Figure 4-2) the pressure in the tank is reduced and the gas desorbs. The rate of desorption was measured by the polarographic probes and the profile processed using Equation 4-8.

4.4.2. Measurements in dispersion

The addition of a small concentration of particles to a batch may or may not change the interfacial area in dispersion. The effect of the particles on interfacial area was measured by the chemical method. When the effect was established, volumetric mass transfer coefficients were measured in the stirred cell as well as the agitated tank by a variety of methods.

4.4.2.1 Measurements by the chemical sulphite method

Once the effect of particle addition on the reaction kinetics is known, it is possible to measure the effect of particle presence on dispersion interfacial area using the sulphite method. The absorption rate was measured in the fast chemical reaction region for a batch without particles, and then after the addition of particles. The experiment was

- Gas interchange method

$k_L a$ was measured in the cell by the start-up variety of the gas interchange method (refer to Section 3.1.1.2). Figure 4-13 illustrates the procedure used to make measurements. The batch was saturated with nitrogen after which the aeration was ceased and the gas bubbles were allowed to leave the system. The nitrogen gas was then interchanged for either oxygen or hydrogen gas.

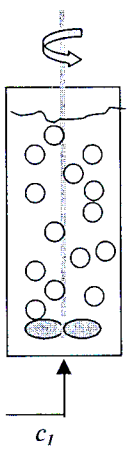
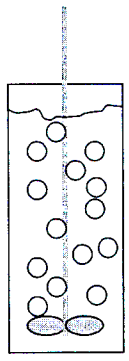
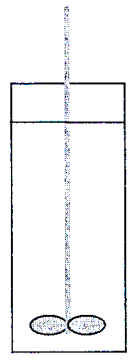
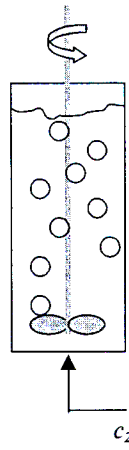
1 First steady state with gas $c = c_I^g$	2 Dispersion and agitation ceased	3 Batch is degassed	4 Interchange to gas $c = c_2^g$
<ul style="list-style-type: none"> • Stirrer: On • Gas c_I^g: On • Gas c_2^g: Off 	<ul style="list-style-type: none"> • Stirrer: Off • Gas c_I^g: Off • Gas c_2^g: Off 	<ul style="list-style-type: none"> • Stirrer: Off • Gas c_I^g: Off • Gas c_2^g: Off 	<ul style="list-style-type: none"> • Stirrer: On • Gas c_I^g: Off • Gas c_2^g: On
			

Figure 4-13: Experimental implementation of the start-up method for the measurement of $k_L a$

The following equation is valid if perfect mixing is assumed in the liquid phase:

$$\frac{dc_L}{dt} = k_L a (c_L^* - c_L)$$

Equation 4-10

The solution is given by:

Depending on the state of SV1 and SV2 (Figure 4-2), the outlet of the tank was opened to one of two tubes installed in the manostat. The first is effectively open to atmospheric pressure whereas the second is submersed below 2 m of water. Using this arrangement, it is possible to perform a very quick pressure step in the tank. Opening of SV2 for a short while provides a “boost” to enable rapid pressure up steps. Simultaneous transport of nitrogen occurs when experiments are made with air. This was not a consideration in this study as absorption of pure oxygen was measured.

Figure 4-10 shows that it is sufficient to describe the dynamics of the probes used in this study as a first-order response. Linek et al. (1996) show that a simple model of perfect mixing in both phases is sufficient to obtain correct values for $k_L a$. Fuchs et al. (1971) present such a simple model using the following equations for the mass transfer process:

$$\frac{dc_L}{dt} = k_L a (c_L^{*2} - c_L)$$

Equation 4-12

The first order response of the probe is given by:

$$\frac{dc_P}{dt} = k_m (c_L - c_P),$$

Equation 4-13

where c_P is the concentration as read by the probe (dynamically different from c_L , which is the actual concentration) and k_m is the first order response constant. Introducing the following definitions:

$$Y_m = \frac{c_L^{*2} - c_L}{c_L^{*2} - c_L^{*1}} \quad Y_P = \frac{c_P^{*2} - c_P}{c_P^{*2} - c_P^{*1}},$$

where c_L^{*1} and c_P^{*1} are the saturation values at the first pressure. c_L^{*2} and c_P^{*2} represent the saturation values at the second pressure. Since these are steady state values:

The vessel pressure is set to a value approximately 20% higher than atmospheric pressure using the manostat. The gas flow is set to a high value as is the stirrer speed to ensure that the batch is saturated. The value, c^{*1} , is recorded.

A reading after a known period of aeration was taken

The experimental conditions of flow and stirrer speed are set and the pressure decreased instantly to atmospheric pressure using SV1. After a known time of aeration at the new pressure, the flow and stirring is ceased and the concentration is recorded ($c_{\Delta t}$).

A concentration reading at the new steady-state is required

The stirring and agitation is resumed at the high values in order to obtain the saturation value at the new pressure (c^{*2}).

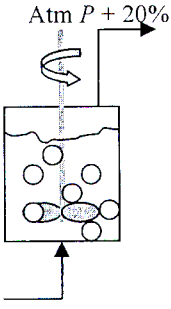
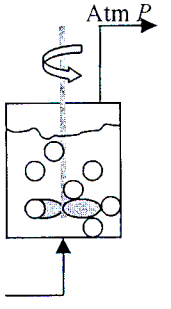
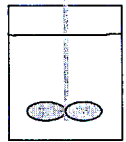
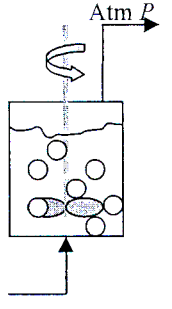
1 Batch saturated at P_1	2 Pressure step to P_2 (time = 0)	3 Reading at P_2 (time = Δt)	4 Batch saturated at P_2
Record saturation value c^{*1} by the procedure given in Figure 4-16	Set experimental conditions, make P step and begin recording aeration time Δt	Stop aeration and stirring. Record $c_{\Delta t}$ by the procedure given in Figure 4-16	Record saturation value c^{*2} by the procedure given in Figure 4-16
 <ul style="list-style-type: none"> • Stirrer speed: High • Gas flow: High 	 <ul style="list-style-type: none"> • Stirrer speed: Experimental conditions • Gas flow: Experimental conditions 	 <ul style="list-style-type: none"> • Stirrer speed: Off • Gas flow: Off 	 <ul style="list-style-type: none"> • Stirrer speed: High • Gas flow: High

Figure 4-15: Illustration of the discrete dynamic method for measurement of $k_L a$
(see Figure 4-16 for procedure for measurement of overall dissolved gas concentration)

$$k_L a = \frac{\ln \frac{c^{*2} - c^{*1}}{c^{*2} - c_{\Delta t}}}{t}$$

Equation 4-18

4.5. *List of experiments*

The data points reported in this study were confirmed to be repeatable during the experimental program. Each point was measured at least two times. The data are reported in Chapter 5.

The effect of particles on reaction kinetics and interfacial area was measured by chemisorption experiments (Table 4-4). 0.8 M sodium sulphite solution was used to absorb oxygen gas at 30 °C. Experiments were made in the stirred cell as well as the agitated tank. The absorption rate was varied by changing the impeller speed and catalyst concentration.

Table 4-4: List of chemisorption experiments made in this study to measure the effect of particles on reaction kinetics and interfacial area

Experiment	Apparatus	Particles/ g //
Effect of particles on kinetics	Stirred cell	0
		0.1
		1
Effect of particles on interfacial area	Agitated tank	0
		0.1
		1

Dispersion sorption experiments were made in the stirred cell (Table 4-6) and the agitated tank for various impeller speeds. The gas flow rate was also varied for the agitated tank experiments.

Table 4-6: List of experiments made in this study to determine the effect of particle addition on n in the stirred cell

Method	Apparatus	Liquid	T /°C	Gas	Particles/ g /l
Start-up interchange	Stirred cell	Water	20	O ₂	0
				H ₂	0
				O ₂	1
				H ₂	1
Start-up interchange	Stirred cell	Sulphate	20	O ₂	0
				H ₂	0
				O ₂	1
				H ₂	1

Dispersion sorption experiments were also made in the agitated tank (Table 4-7). The DPM measurements were made by both pressure up and down steps. Besides each point being repeated, the DPM measurements were made with two probes installed in the apparatus. The experiments were performed on two different batches of water for the DPM and discrete dynamic methods.

4.6. *Chapter summary*

This chapter described in detail the apparatuses and chemicals used in this study as well as implementation of the various experimental methods. Sorption experiments were made in a stirred cell apparatus as well as an agitated tank. The features of the apparatuses were given as well as the construction detail.

The characteristics and construction of the analytical technique for the measurement of dissolved gas concentration were described at length. The polarograms were measured to ensure that the probes were operating in the limiting diffusion current region. Signal linearity was excellent for both increasing and decreasing concentration changes. 95% of the dynamic response of the probes was sufficiently described as a first order response. The time constant for the O₂ probe was 1.25 s and the H₂ probe's constant was 2 s, which makes them suitable to measure rapid changes in concentration.

Following a detailed review of available experimental methods, the chemical sulphite method was used to determine the effect of particles on the kinetics of the sulphite reaction in the stirred cell. The effect of particles on dispersed phase interfacial area was also measured by the sulphite method; this time however, in the agitated tank.

Surface desorption experiments were made in both the stirred cell and the agitated tank. The gas interchange method (stirred cell) and the DPM (agitated tank) were implemented in order to determine k_L . Measurements in bubble dispersion for both apparatuses were made using the same methods, however, $k_L a$ was determined. The discrete dynamic method was also used for agitated tank experiments.

The comprehensive experimental program was listed in this chapter and are reported and discussed in the ones that follow.

Chapter 5 Results

Gas-liquid mass transfer rates were measured in the stirred cell and agitated tank described in Figure 4-1 and Figure 4-2 (respectively). Both apparatuses were used to make the following types of measurements:

- Absorption rates with simultaneous chemical reaction
- Flat surface desorption rates
- Sorption rates in bubble dispersion

The experimental methods are described in Chapter 4 and the results are discussed in Chapter 6.

5.1. *Gas absorption with chemical reaction*

The chemical sulphite method was used to measure the effect of solid particles on the interfacial area. The methods were implemented as described in Section 4.4.

5.1.1. Surface absorption – mass transfer cell

The flat surface absorption measurements were made in the fast reaction regime to confirm that the presence of particles does not affect the kinetics of the sulphite reaction. The measured stirred cell absorption rates and those calculated from are Equation 4-6 given in Table 5-1.

5.1.2. Measurements in dispersion – agitated tank

Specific gas absorption rates in the agitated tank were measured in dispersion to determine the effect of the particles on interfacial area.

Absorption rates into 0.8 M Na₂SO₃ solution are given in Table 5-2. Absorption rates in the presence of 1 g /l of activated carbon are given in Table 5-3. The experimental data were recalculated to a pH of 8.5 and CoSO₄ concentration of 1 M using Equation 4-9.

Table 5-2: O₂ absorption rate into 0.8 M sulphite solution (without activated carbon particles) measured in the agitated tank at 30 °C and a gas flow of 1 l /min

F /rpm	pH	CoSO₄ × 10⁴ /M	N_{exp} × 10⁷ /kmol·m ⁻³ ·s ⁻¹	N_{RS}^{Equation 4-9} × 10⁵ /kmol·m ⁻³ ·s ⁻¹
331	8.62	0.5	1.997	2.690
331	8.60	0.5	2.022	2.756
331	8.53	0.5	1.908	2.682
451	8.38	0.5	4.552	6.916
451	8.25	0.5	4.539	7.377
451	8.58	0.5	5.467	7.503
601	8.55	0.5	11.281	15.705
601	8.51	0.5	10.849	15.436
330	8.54	1.0	2.655	2.633
330	8.28	1.0	2.277	2.581
450	8.43	1.0	5.960	6.240
600	8.32	1.0	13.638	15.126

Table 5-4: Mass transfer coefficients measured in water at 20°C (with and without 1 g /l carbon) by surface desorption in the stirred cell

<i>F</i> /rpm	$k_L (\text{m}\cdot\text{s}^{-1}) \times 10^4$ (oxygen)			$k_L (\text{m}\cdot\text{s}^{-1}) \times 10^4$ (hydrogen)		
	Without carbon	With carbon	$\frac{k_L^{with}}{k_L^{without}}$	Without carbon	With carbon	$\frac{k_L^{with}}{k_L^{without}}$
150	0.30	-	-	0.50	-	-
250	0.63	2.59	4.10	0.94	3.70	3.96
350	0.90	3.43	3.80	1.45	5.03	3.48

Table 5-5: Mass transfer coefficients measured in water at 30°C (with and without 1 g /l carbon) by surface desorption in the stirred cell

<i>F</i> /rpm	$k_L (\text{m}\cdot\text{s}^{-1}) \times 10^4$ (oxygen)			$k_L (\text{m}\cdot\text{s}^{-1}) \times 10^4$ (hydrogen)		
	Without carbon	With carbon	$\frac{k_L^{with}}{k_L^{without}}$	Without carbon	With carbon	$\frac{k_L^{with}}{k_L^{without}}$
50	0.16	0.43	2.80	0.26	0.61	2.35
100	0.25	0.73	2.91	0.40	1.10	2.78
150	0.35	1.10	3.15	0.52	1.55	2.95
200	0.42	1.31	3.14	0.64	1.90	2.99
250	0.52	1.58	3.05	0.79	2.37	2.99
300	0.60	1.98	3.33	0.96	2.69	2.82

5.2.2. Agitated tank

The discrete dynamic method was used to measure flat surface desorption from water at 20 °C. Mass transfer coefficients in the absence and presence of 1 g /l activated carbon particles are presented in Table 5-8.

Table 5-8: Mass transfer coefficients measured in water at 20°C (with and without 1 g /l carbon) by surface desorption in the agitated tank

<i>F</i> /rpm	$k_L (\text{m}\cdot\text{s}^{-1}) \times 10^2$ (oxygen)			$k_L (\text{m}\cdot\text{s}^{-1}) \times 10^2$ (hydrogen)		
	Without carbon	With carbon	$\frac{k_L^{with}}{k_L^{without}}$	Without carbon	With carbon	$\frac{k_L^{with}}{k_L^{without}}$
300	1.85	2.96	1.60	3.06	4.38	1.43
420	2.42	4.13	1.71	4.23	5.78	1.37

5.3. Dispersion

Physical desorption measurements in dispersion were made in the stirred cell as well as the agitated tank.

5.3.1. Stirred cell

The gas interchange method was used to measure O₂ and H₂ desorption rates into water and 0.8 M Na₂SO₄ solution. Table 5-9 and Table 5-10 give volumetric mass transfer coefficients measured at 20 °C for the liquid phases before and after the addition of 1 g /l of activated carbon. The experimental method is described in Chapter 4.

Table 5-11: k_La values for O₂ in water (batch 1) measured by the DPM in the agitated tank. Two different types of probes were used.

Gas flow (l/min)	F /rpm	$k_La^{up\ step} (s^{-1})$ $\times 10^2$ (oxygen)		$k_La^{down\ step} (s^{-1})$ $\times 10^2$ (hydrogen)	
		Pt	Au	Pt	Au
		cathode	cathode	cathode	cathode
3	330	1.081	1.032	1.334	1.301
	600	3.770	3.901	4.252	4.138
	860	6.163	6.070	8.000	7.434
	1130	12.983	11.019	16.865	16.050
6	330	1.041	1.002	1.050	1.032
	600	4.020	3.991	3.876	3.812
	860	8.555	8.391	8.672	8.215
	1130	16.479	15.169	17.145	16.260
9	330	1.384	1.415	1.458	1.429
	600	4.141	4.170	4.369	4.282
	860	8.611	8.330	9.034	8.780
	1130	14.308	13.160	16.591	15.982

Table 5-13: k_La values for O₂ and H₂ in water (batch 2) measured by the pressure up-step DPM in the agitated tank (with and without the addition of 1 g /l activated carbon)

Gas flow (l/min)	F /rpm	k_La (s ⁻¹) × 10 ² (oxygen)		k_La (s ⁻¹) × 10 ² (hydrogen)	
		Without carbon	With carbon	Without carbon	With carbon
3	300	0.570	0.650	0.630	0.810
	420	1.090	1.130	1.380	1.550
	600	2.300	2.520	2.960	2.350
	860	6.490	7.240	6.380	6.960
6	300	0.820	0.970	1.100	1.340
	420	1.490	1.700	1.960	2.190
	600	3.680	4.140	4.230	4.610
	860	8.750	9.540	9.060	8.910
9	300	1.150	1.340	1.420	1.680
	420	2.040	2.280	2.430	2.790
	600	4.660	5.080	4.760	5.290
	860	10.170	11.640	10.340	6.480

Table 5-15: k_La values for O₂ and H₂ in water (batch 1) measured by the discrete dynamic method in the agitated tank (with and without the addition of 1 g/l activated carbon)

Gas flow (l/min)	F /rpm	k_La (s ⁻¹) × 10 ² (oxygen)		k_La (s ⁻¹) × 10 ² (hydrogen)	
		Without carbon	With carbon	Without carbon	With carbon
3	300	0.469	0.548	0.667	0.760
	420	0.964	1.049	1.353	1.444
	600	2.140	2.474	2.880	3.271
	860	5.403	6.767	6.589	7.149
6	300	0.692	0.866	0.944	1.137
	420	1.345	1.553	1.602	2.034
	600	2.770	3.531	3.732	4.325
	860	6.680	8.312	7.762	9.335
9	300	0.887	1.184	1.087	1.373
	420	1.682	2.101	2.014	2.254
	600	3.473	4.079	3.970	4.647
	860	7.275	9.065	8.418	9.603

performance. Preparation of the probe and fitment of the membrane is a delicate exercise. These actions were necessary when a decline in the probe performance was noted.

The linearity of the probe signals was tested for both hydrogen and oxygen probes. The results (Section 4.3.4) show that the probes used responded linearly to both increases and decreases in concentration. The dynamic response of the probes was also successfully modelled as a first order response. Up to 95 % of the probe signal can be represented as a first order response (see Section 4.3.5). The time constant for the O₂ probe was 1.25 s and the H₂ probe's constant was 2 s, which makes them suitable to measure rapid changes in concentration. The model was used to extract the concentration-time profile required to calculate k_La values by the dynamic methods.

The pressure dependence displayed by the probes was a concern. The feature (described in Section 4.3.6) was caused by deflection of the membrane during the rapid pressure steps made when implementing the DPM. The measured profile is distorted and contributed to the uncertainty observed in the DPM results.

6.2. *Effect of particles on interfacial area*

Since volumetric mass transfer coefficients (k_La) were measured in dispersion, it is important to establish the effect of particle addition on the specific interfacial area (a). Without quantifying this effect, it is unclear whether an increase in k_La can be attributed to an enhancement of k_L or a .

The chemical sulphite method is a technique that can be used to determine the effect. In order to implement the chemical method correctly the first step is to measure the effect of the solid particles on the reaction kinetics of the sulphite reaction. Extensive studies on the subject of oxygen absorption into sodium sulphite solution in the presence of cobalt catalyst were made by Linek and Vacek (1981) and Linek et al. (2005a). The theory of absorption with fast chemical reaction is discussed in Section 2.4. By using appropriate cobalt catalyst concentration, the oxygen absorption rate into sulphite solution occurs at large values of the enhancement factor. At sufficiently high values, the absorption rate does not depend on the physical mass transfer

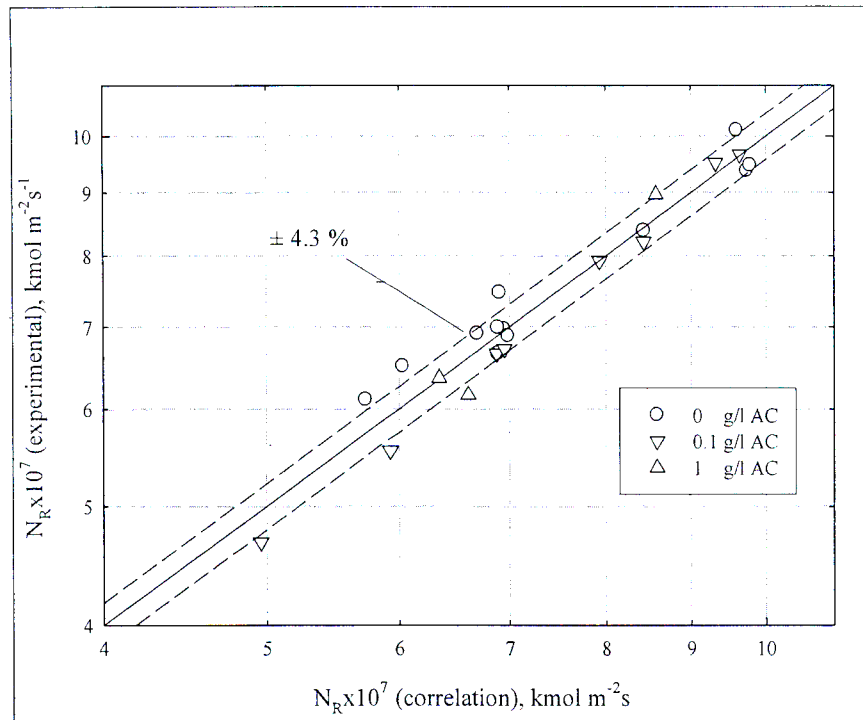


Figure 6-1: Oxygen absorption rate calculated from Equation 4-6 compared with those measured in the stirred cell into a 0.8 M Na_2SO_3 solution (with and without particles)

6.2.2. Specific interfacial area of dispersion

The significance of the previous result is apparent when considering oxygen-sulphite dispersion with fine particles. It has been established that the particles do not affect the kinetics of the reaction and that the hydrodynamic effect is suppressed if the reaction rate is high. Consequently, changes in the oxygen mass transfer rate into the sulphite solution in the fast reaction regime are due to changes of interfacial area only.

Figure 6-1 also confirms that a is not affected by the presence of particles. However, this result is only valid for a flat mass transfer area. In dispersion the interface region is continuously regenerated and the result has to be confirmed. Both absorption rates measured with and without addition of activated carbon were recalculated by this relationship to the conditions of $\text{pH} = 8.5$ and catalyst concentration of 1 M and are compared in Figure 6-2. The experimental method and recalculation procedure using Equation 4-9 are given in Section 4.4.2.1. There is no significant difference between

N₂. The experiments were conducted in a coalescent batch (water) as well as in a non-coalescent batch (0.8 M sodium sulphate solution).

Desorption rates were measured at various impeller speeds up to a maximum of 350 rpm. Wave formation was observed above 350 rpm and the surface could no longer be assumed to be flat. The experimental data are given in Table 5-4 to Table 5-7. The data were fitted to the following equation (Kordač and Linek, 2006):

$$k_L = \alpha_1 f^{\alpha_2} D^n$$

Equation 6-1

The parameters obtained by fitting the experimental results to Equation 6-1 are given in Table 6-1. With the exception of the value of 0.78, the exponent of the diffusion coefficient (n) before the addition of the solid phase is approximately $\frac{2}{3}$ (within 10%). n reduces to $\frac{1}{2}$ after the particles are added (also within 10%). The data for water and sulphate are plotted in Figure 6-3 to Figure 6-6. The values predicted by the correlation are also shown in the graphs.

Table 5-4 to Table 5-7 clearly show the mass transfer enhancement after the addition of solid particles. These enhancements are well in excess of 200%. The mass transfer coefficients measured at 20 °C are higher than those at 30 °C due to differences in the agitator used.

Table 6-1 also shows the relationship between k_L and the impeller frequency, f . For the data measured at 30 °C α_2 , the exponent of f , is on average 0.72. The relationship between f and the energy dissipation intensity is approximated as follows:

$$e \propto f^3$$

Equation 6-2

This implies that for the 30 °C data that $k_L \propto e^{0.24}$. This is in excellent agreement with the value of $\frac{1}{4}$ predicted for the exponent of e by Lamont and Scott (1970) (see Equation 2-27 and Equation 2-29). The exponent for the 20 °C data is 0.34, although

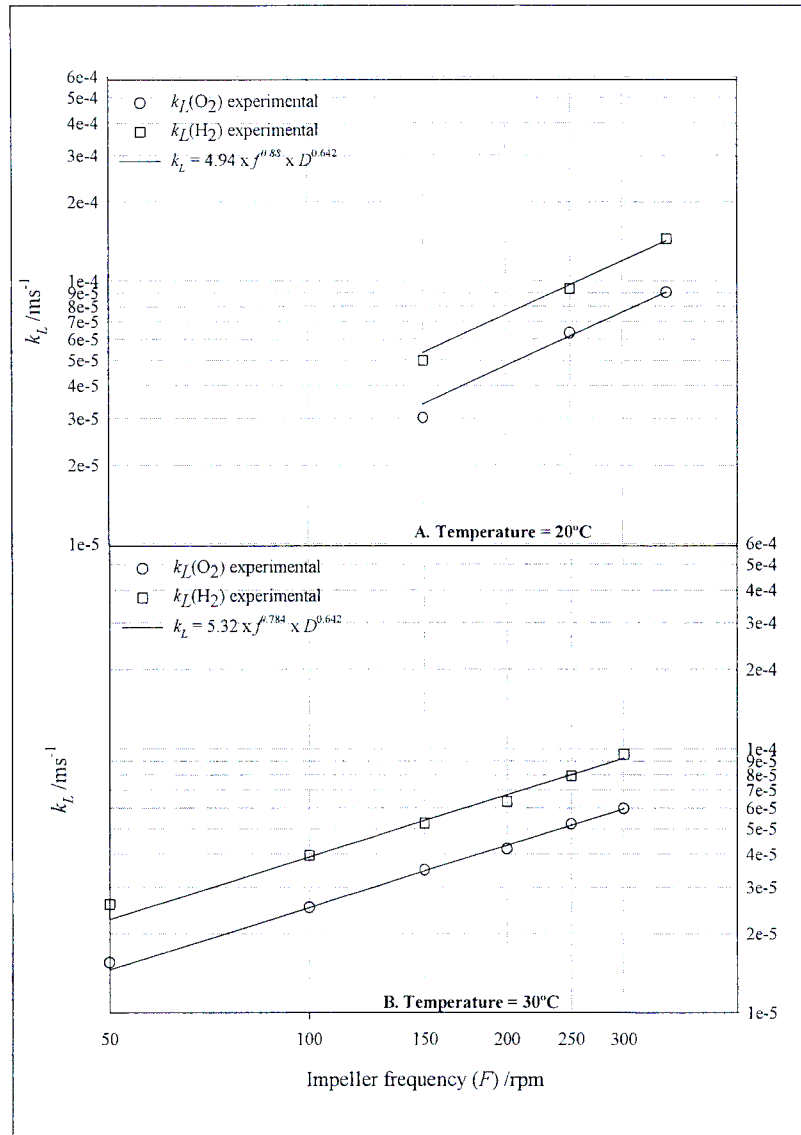


Figure 6-3: Mass transfer coefficients measured in water by surface desorption in a stirred cell

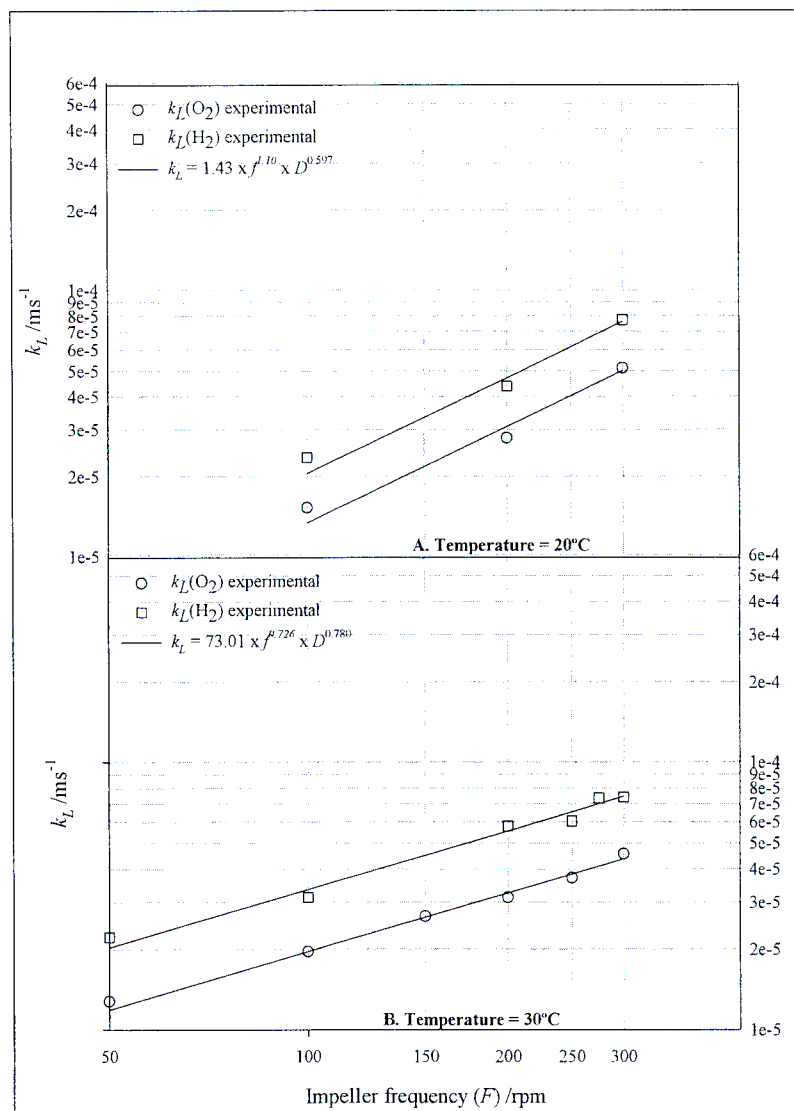


Figure 6-5: Mass transfer coefficients measured in 0.8 M sodium sulphate solution by surface desorption in a stirred cell

The results for water are summarized in the Table 5-8. The desorption rate of gases was measured to avoid the supersaturation effect. The desorption rate is very low at low impeller frequencies due to the large batch size (5.9 l). When the impeller rate was larger than 420 rpm, the surface could no longer be assumed flat. The measurements were, therefore, made at 300 rpm and 420 rpm only.

The values of n calculated from the data are given in Table 6-2. As observed for the stirred cell experiments, the value of n decreases from approximately $\frac{2}{3}$ to $\frac{1}{2}$.

Table 6-2: The value of n calculated from the surface absorption experiments

Liquid batch	F (/rpm)	n
Water	300	0.610
	420	0.681
Water + Carbon	300	0.475
	420	0.410

6.4. Dispersion

6.4.1. Stirred cell

Volumetric mass transfer coefficients were measured for O_2 and H_2 by the gas interchange method discussed in Chapter 4. $k_L a$ values are presented in Table 5-9 and Table 5-10 for a gas velocity of 2 l/min. Measurements were made in both coalescing and non-coalescing liquid batches (water and 0.8 M sodium sulphate, respectively) at 20 °C. Due to the principle of the method, the pressure dependence of the polarographic probes did not distort the results.

It is noted from these measurements that:

- Particles enhance $k_L a$ in dispersion.
- For a particular batch, the absorption rate increases to the same extent for O_2 and H_2 after the addition of solid particles.

Equation 6-3 resembles empirical correlations which have often been used (Linek et al., 1987 and Fújasová et al., 2007) to correlate the volumetric mass transfer coefficient in aerated stirred tank reactors with the specific power input and the superficial gas velocity. The measured data were correlated to the following equation:

$$k_L a = (A_1 + A_2 f^{A_3}) Sc^{-n}$$

Equation 6-4

The form of the correlation reflects that the agitated vessel operates as a bubble tank with non-zero $k_L a$ value at no agitation and that all the experiments were performed at a single gas velocity of 2 l/min. Equation 6-4 fits the experimental data well as shown in Figure 6-7 and Figure 6-8 (parameters are given in Table 6-3).

Table 6-3: Parameters of Equation 6-4 fitted to the measured data

Liquid batch	A_1	A_2	A_3	n
Water	0.062	0.0340	2.15	0.622
Water + Carbon	0.141	0.01430	2.34	0.531
Sulphate	24.39	0.3260	3.33	0.626
Sulphate + Carbon	7.131	0.1821	2.86	0.497

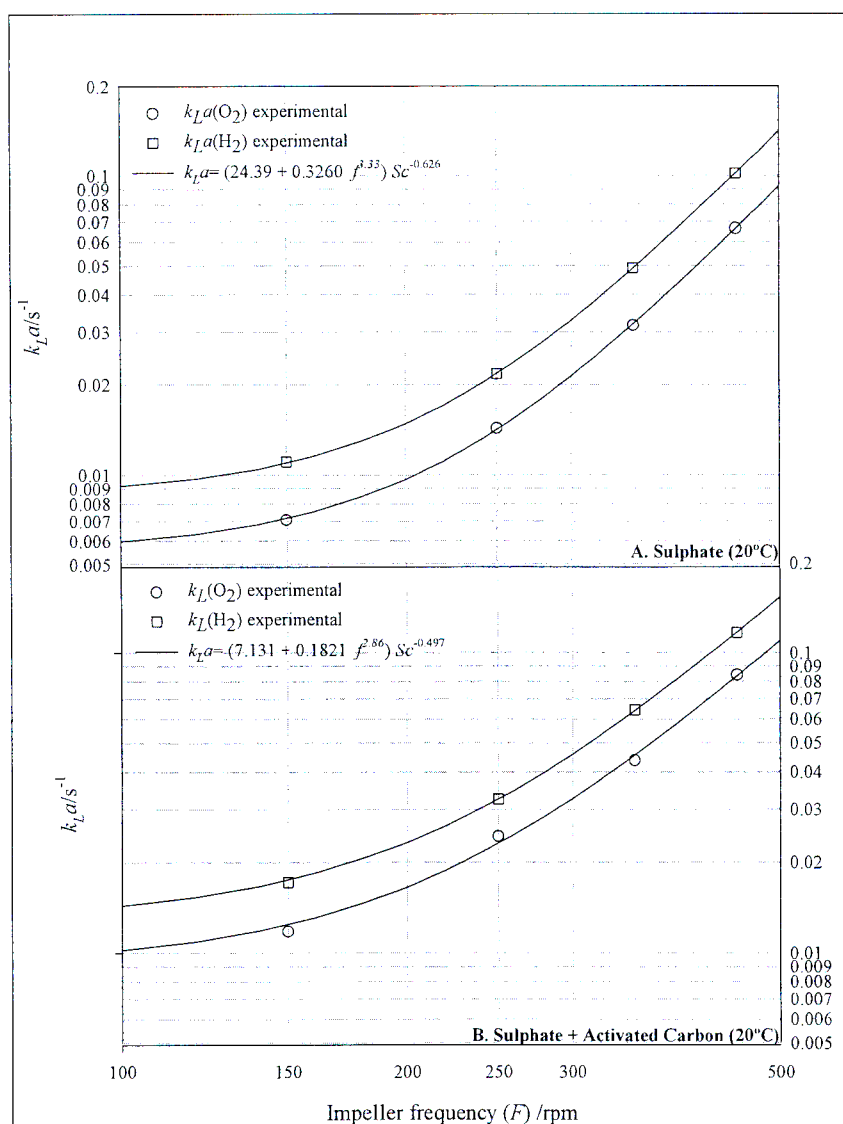


Figure 6-8: Volumetric mass transfer coefficients measured in sulphate solution-gas dispersion in a stirred cell at 20 °C

Values of the exponent of the Schmidt number (which is $-n$) are close to those theoretically predicted for contaminated and mobile surfaces. Values of 0.622 and 0.626 are calculated for water and sulphate, respectively (compared to the theoretical value of $\frac{2}{3}$ for a rigid surface). The exponent reduces to 0.531 and 0.497 after the addition of 1 g /l of activated carbon to water and sulphate, respectively. These values compare well with the theoretical prediction of $\frac{1}{2}$ for a mobile interface. The surface absorption measurements have confirmed that n reduces from $\frac{2}{3}$ to $\frac{1}{2}$ after the addition of 1 g /l of activated carbon. The agitated cell experiments extend the observation to agitated dispersion.

$$\frac{(k_L)_{SC}}{(k_L)_{pure}} = \frac{1}{1.25 + 0.073\pi}$$

Equation 6-5

For $\pi > 16 \text{ mN}\cdot\text{m}^{-1}$

$$\frac{(k_L)_{SC}}{(k_L)_{pure}} = 0.41$$

Equation 6-6

The results given in the figure show that the decrease of mass transfer coefficients due to presence of surfactants roughly coincide with the increase of mass transfer coefficients due to removal of the surfactants by adsorption onto particles.

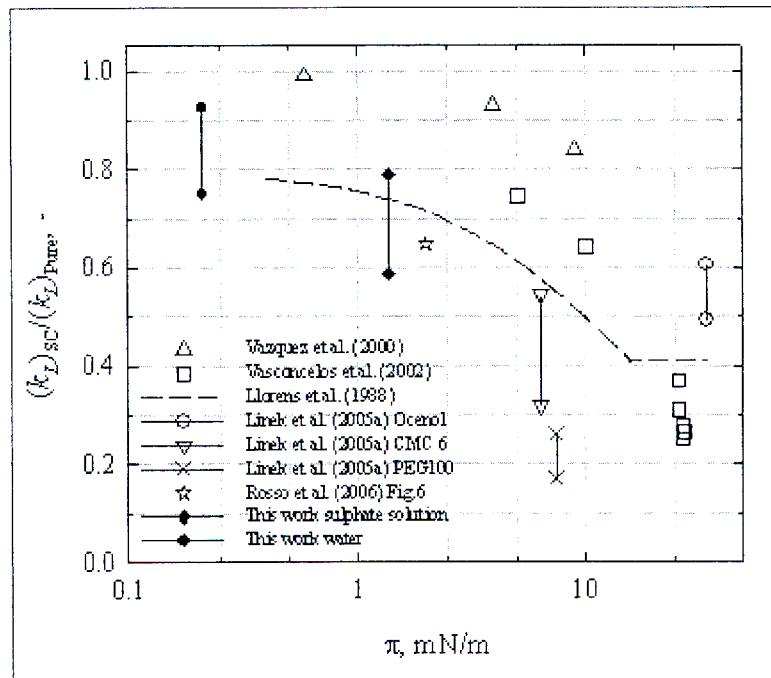


Figure 6-9: Comparison of the effect of particle addition using Llorens et al. (1988) surface pressure interpretation

to probe pressure dependence and the time constant of the probe being comparable to the mass transfer rate.

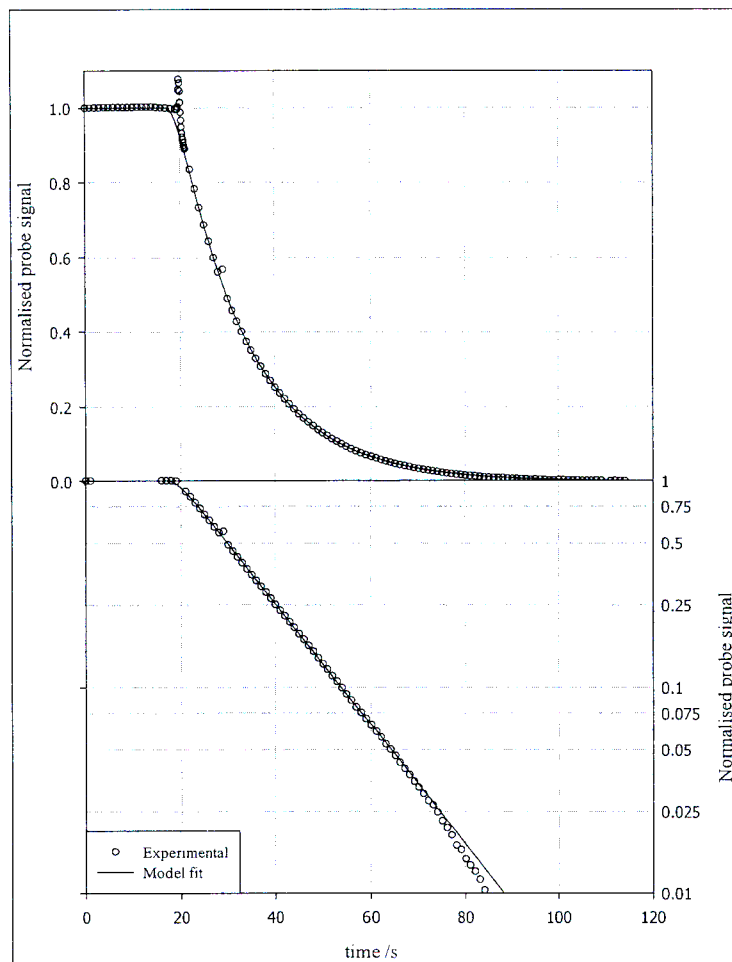


Figure 6-10: Graphs to show the effect of the pressure step and the model fit to the data

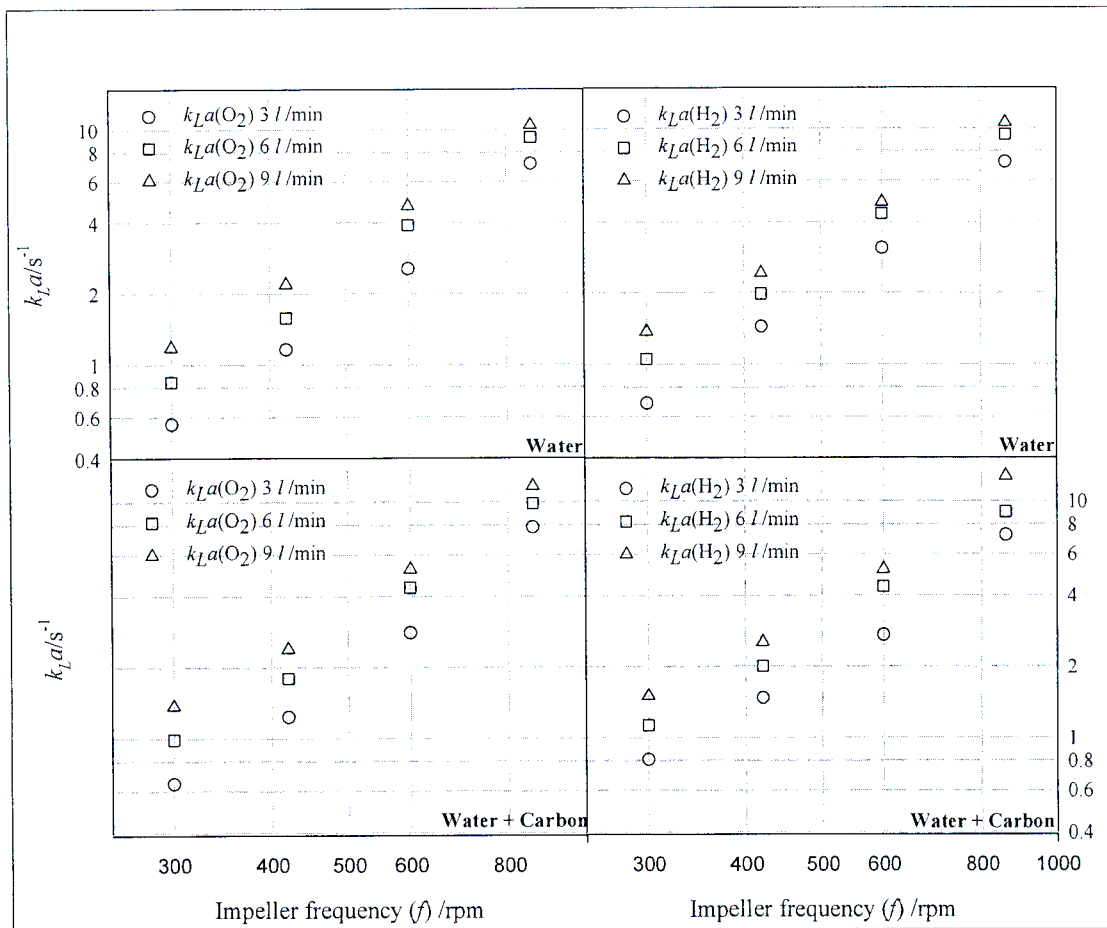


Figure 6-11: Volumetric mass transfer coefficients measured in the agitated tank by the dynamic pressure method

6.4.2.2 Discrete dynamic method

Two batches of measurements were made by the discrete dynamic method in water. The method allows for the overall $k_L a$ to be measured from three concentration readings. The dynamics of the probe are not important and the pressure dependence was accounted for by recording the step change in signal due to the pressure step. Despite showing excellent repeatability, this did not sufficiently account for the pressure dependence as the movement of the membrane is not exactly reversible. As with the DPM measurements, the precision of the data presented in Table 6-5 and Figure 6-12 is also not sufficiently high to measure the effect of solid particles. The measurement is made while the dispersion was still developing and this is believed to have influenced the results.

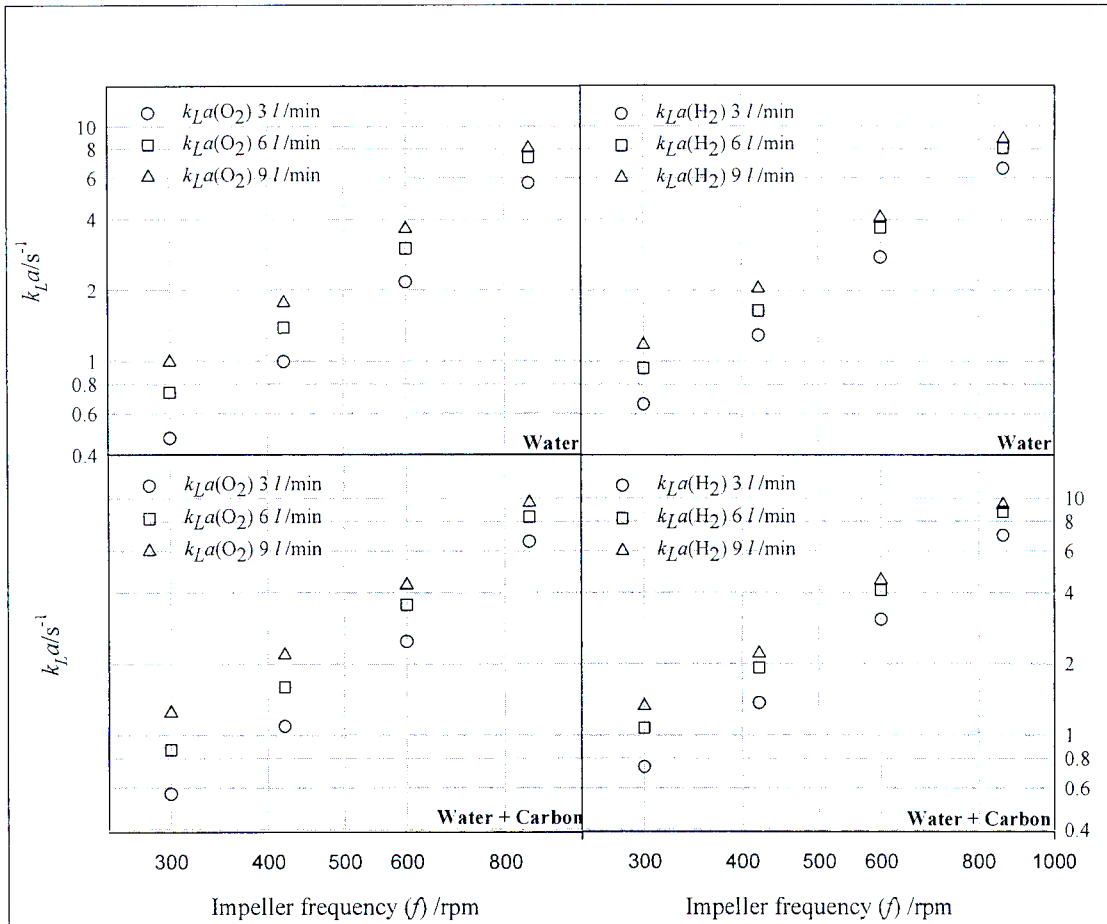


Figure 6-12: Volumetric mass transfer coefficients measured in the agitated tank by the discrete dynamic method (average of two batches)

6.5. Chapter summary

The O₂ and H₂ polarographic probes used in this study were rigorously characterized. The polarograms were measured to ensure that the probes were operating in the limiting diffusion current region. Signal linearity was excellent for both increasing and decreasing concentration changes. 95% of the dynamic response of the probes was sufficiently described as a first order response. The time constant for the O₂ probe was 1.25 s and the H₂ probe's constant was 2 s, which makes them suitable to measure rapid changes in concentration. $k_L a$ measurement by the gas interchange method was successfully performed. These probes were, however, found to be affected by pressure steps due to small movements of the membrane. The pressure dependence results in a distorted profile which severely affects their precision. The effect of the reduction of n is within the uncertainty of the measurements.

Chapter 7 Conclusions

Mass transfer models make assumptions about fluid flow and diffusion. The exponent of the diffusion coefficient, n , predicted by these models depends on whether fluid flow in the interface region is assumed to be opposed or free. The presence of surfactants in the interface region results in opposed flow and the exponent is predicted to be $\frac{2}{3}$. Removal of these impurities results in the reduction of n to a value of $\frac{1}{2}$.

The enhancement of mass transfer rates in the presence of micro particles is traditionally explained by a “shuttle” mechanism. However, Kaya and Schumpe (2005) present evidence to show that the presence of particles removes the impurities, which are normally present in the liquid phase and allows the true mass transfer coefficient to be measured. The precise measurement of mass transfer coefficients of gases of significantly different diffusion coefficients will reveal the effect of particle addition on n .

A review of experimental methods to measure mass transfer rates and interfacial area was made. The gas-interchange and pressure step methods were implemented in a stirred cell (500 ml) and an agitated tank (5.9 l). Polarographic probes were used to measure changes in dissolved gas concentration. These probes were characterised and the dynamic response of the probes is well understood. The signal of the probes was also found to be pressure dependent.

Chapter 8 References

Akita, K., (1981), "Diffusivities of gases in aqueous electrolyte solutions," *Industrial Engineering Chemistry Fundamentals*, Vol. 20, pp. 89-94.

Alper, E., Wichtendahl and B., Deckwer, W.-D., (1980), "Gas absorption mechanism in catalytic slurry reactors," *Chemical Engineering Science*, Vol. 35, pp. 217–222.

Alves, S.S., Maia and C.I., Vasconcelos, J.M.T., (2004), "Gas-liquid mass transfer coefficient in stirred tanks interpreted through bubble contamination kinetics," *Chemical Engineering and Processing*, Vol. 43, pp. 823–830.

Beenackers, A.A.C.M. and van Swaaij, W.P.M., (1993), "Mass transfer in gas-liquid slurry reactors," *Chemical Engineering Science*, Vol. 48, pp. 3109–3139.

Brian, P.L.T., Vivian, J.E. and Matiatos, D.C., (1967), "A criterion for supersaturation in simultaneous gas absorption and desorption," *Chemical Engineering Science*, Vol. 22, p. 7-10.

Calderbank, P.H. and Moo-Young, M.B., (1961), "The continuous phase heat and mass-transfer properties of dispersions," *Chemical Engineering Science*, Vol. 16, pp. 39-54.

Kaya, A., Schumpe, A., (2005). "Surfactant adsorption rather than "shuttle effect"? ,” *Chemical Engineering Science*, Vol. 60, pp. 6504 – 6510.

Kluytmans, J.H.J., van Wachem, B.G.M., Kuster, B.F.M. and Schouten, J.C., (2003), "Mass transfer in sparged and stirred reactors: influence of carbon particles and electrolyte," *Chemical Engineering Science*, Vol. 58, pp. 4719 – 4728.

Kordač, M. and Linek, V., (2006), "Mechanism of enhanced gas absorption in presence of fine solid particles. Effect of molecular diffusivity on mass transfer coefficient in stirred cell," *Chemical Engineering Science*, Vol. 61, pp. 7125-7132.

Lamont, J.C. and Scott, D.S., (1970), "An eddy cell model of mass transfer into the surface of a turbulent liquid," *A.I.Ch.E. Journal*, Vol. 16, pp. 513-519.

Linek, V., Kordač, M. and Soni, M., (2008), "Mechanisms of gas absorption enhancement in presence of fine solid particles in mechanically agitated gas-liquid dispersion. Effect of molecular diffusivity," *Chemical Engineering Science*, doi: 10.1016/j.ces.2008.06.23.

Linek, V. and Vacek, V., (1981), "Chemical Engineering use of catalyzed sulfite oxidation kinetics for the determination of mass transfer characteristics of gas-liquid contactors," *Chemical Engineering Science*, Vol. 36, No. 11, pp. 1747-1768.

Linek, V., Vacek, V. and Beneš, P., (1987), "A critical review and experimental verification of the correct use of the dynamic method for the determination of oxygen transfer in aerated agitated vessel to water, electrolyte solutions and viscous liquids," *The Chemical Engineering Journal*, Vol. 34, pp. 11-34.

Linek, V., Vacek, V., Sinkule, J. and Beneš, P., Measurement of oxygen by membrane-covered probes: Guidelines for applications in chemical and biochemical engineering, Ellis Horwood, John Wiley and Sons, 1988.

Rosu, M., Marlina, A., Kaya, A. and Schumpe, A., (2008), "Surfactant adsorption onto activated carbon and its effect on absorption with chemical reaction," *Chemical Engineering Science* (in press).

Soni, M., Kordač, M., Linek V., Ramjugernath, D. and Čarsky, M., (2006), "Hydrogen and oxygen probe for measurement of mass transfer coefficients by a dynamic method," Presented at the 2006 South African Institute of Chemical Engineers Conference at Sun City, South Africa.

Vasconcelos, J.M.T., Nienow, A.W., Martin, T., Alves, S.S. and McFarlane, C.M., (1997), "Alternative ways of applying the hydrogen peroxide steady state method of $k_L a$ measurement," *Trans. IChemE*, Vol. 75, Part A, pp. 467-472.

Vasconcelos, J.M.T., Orvalho, S.P. and Alves, S.S. (2002), "Gas-liquid mass transfer to single bubbles: Effect of surface contamination," *A.I.Ch.E. Journal*, Vol. 48, pp. 1145-1154.

Vázquez, G., Cancela, M.A., Riverol, C., Alvarez, E. and Navaza, J.M., (2000), "Application of the Danckwerts method in a bubble column. Effects of surfactants on mass transfer coefficient and interfacial area," *Chemical Engineering Journal*, Vol. 78, pp. 13-19.

Verhallen, P.T.H.M., Oomen, L.J.P., Elsen, A.J.J.M., Kruger, A.J. and Fortun, J.M.H., (1964), "The diffusion coefficients of helium, hydrogen, oxygen and nitrogen in water determined from the permeability of a stagnant liquid layer in the quasi-steady state," *Chemical Engineering Science*, Vol. 39, pp.1535-1541.

Vivian, J.E. and King, C.J., (1964), "The mechanism of liquid-phase resistance to gas absorption in a packed column.," *A.I.Ch.E. Journal*, Vol. 10, pp. 221-227.